Psilocybin-enhanced fear extinction linked to bidirectional modulation of cortical ensembles

Sophie A. Rogers [1, 2, 3]**, Elizabeth A. Heller** [4]**, Gregory Corder** [1, 2, 3] ✉

[1] Department of Psychiatry, Perelman School of Medicine, University of Pennsylvania, Philadelphia, PA, USA

[2] Department of Neuroscience, Mahoney Institute for Neurosciences, Perelman School of Medicine, University of Pennsylvania, Philadelphia, PA, USA

[3] Department of Anesthesiology and Critical Care, Perelman School of Medicine, University of Pennsylvania, Philadelphia, PA, USA

[4] Department of Systems Pharmacology and Translational Therapeutics, Perelman School of Medicine, University of Pennsylvania, Philadelphia, PA, USA

✉ Correspondence: gcorder@upenn.edu (G.C.)

Abstract.

The serotonin 2 receptor (5HT2R) agonist psilocybin displays rapid and persistent therapeutic efficacy across neuropsychiatric disorders characterized by cognitive inflexibility. However, the impact of psilocybin on patterns of neural activity underlying sustained changes in behavioral flexibility has not been characterized. To test the hypothesis that psilocybin enhances behavioral flexibility by altering activity in cortical neural ensembles, we performed longitudinal single-cell calcium imaging in the retrosplenial cortex across a five-day trace fear learning and extinction assay. A single dose of psilocybin induced ensemble turnover between fear learning and extinction days while oppositely modulating activity in fear- and extinction- active neurons. The acute suppression of fear-active neurons and delayed recruitment of extinction-active neurons were predictive of psilocybin-enhanced fear extinction. A computational model revealed that acute inhibition of fear-active neurons by psilocybin is sufficient to explain its neural and behavioral effects days later. These results align with our hypothesis and introduce a new mechanism involving the suppression of fear-active populations in the retrosplenial cortex.

Introduction.

Neuropsychiatric disorders characterized by inflexible associative learning, such as depression, anxiety, substance use-disorders, and post-traumatic stress disorder, affect over 350 million people worldwide[1]. Serotonergic psychedelics, including psilocybin, demonstrate remarkable transdiagnostic potential across these disorders[2]. After only a single dose, many patients report long-lasting improvements in depression and SUDs, as well as overall well-being *for up to a year*—a time-span implicating the involvement of cortically mediated long-term memory[3-6]. Therapeutic-like effects also have been observed in rodent models in many behavioral studies[7-15], enabling the study of the neural mechanisms of psilocybin-enhanced mental health outcomes in mice.

Psilocybin is a naturally occurring compound found in hundreds of species of mushroom. Upon first pass metabolism, psilocybin is dephosphorylated into its active metabolite psilocin – a potent serotonin receptor agonist[16,17]. While psilocybin's subjective effects tend to be accompanied by feelings of extreme "bliss", "unity", and "meaningfulness"[2,18], in a subset of patients, psilocybin can induce anxiogenic and even traumatic experiences, in some cases associated with long-term psychosis and suicidal ideation[19-24]. To develop safe therapies with minimal adverse side-effects, it is critical to identify the relevant neural subpopulations differentially modulated by psilocybin to produce long-lasting therapeutic effects.

Clinical researchers found that therapeutic effects of serotonergic psychedelics in humans are mediated by increased cognitive flexibility following drug experience, a finding recapitulated in rodent models[25-28]. Evidence from human, rodent, and molecular research converges on the hypothesis that psilocybin generates highly plastic brain states conducive to modifying circuits that underlie inflexible, maladaptive behaviors via 5HT2R and TrkB activation[2,17,29-36]. Acute activation of cortical neurons by psychedelics induces synaptic AMPA receptor insertion, BDNF signaling, and consequent dendritic growth[32,35,37,38]. It is unknown how these molecular actions of psilocybin impact information processing in neural ensembles associated with aversive memories and maladaptive behavioral patterns.

The retrosplenial cortex (RSC) is one region where psilocybin may alter information processing in a manner sustaining enhanced behavioral flexibility. The RSC implements a variety of abstract functions[39], including encoding and retrieval of episodic memory[40-51]; imagination of the future[39]; value and context encoding[44-48]; egocentric navigation and reasoning[49,52-54]; and ego dissolution under psychedelics[55]. Chemogenetically inhibiting RSC during reversal learning impairs performance after a rule switch, suggesting RSC activity is crucial for behavioral flexibility[48]. Replay of neural activation in the RSC is also involved in the production, consolidation, and generalization of fear engrams[51]. In another study, Wang et al., 2019 identified a previously silent ensemble recruited in RSC during contextual fear extinction, another form of behavioral flexibility[56]. When the authors optogenetically reactivated this ensemble after re-conditioning, extinction was reinstated, suggesting that excitatory plasticity in the RSC drives fear extinction. The increase in c-FOS-expressing neurons after extinction observed by Wang et al. was recently replicated and shown to be sex-independent[56,57].

Several lines of evidence suggests that psilocybin's effects could in part be mediated by changes in RSC activity. Psilocybin increases c-FOS expression throughout the cortex but idiosyncratically alters neural oscillations specifically in the RSC[58,59]. While 5HT2ARs are distributed throughout cortical L5 pyramidal neurons, the RSC is the only cortical region that also contains 5HT2CRs on pyramidal neurons[60,61]. In humans with depression, functional connectivity between the dorsal raphe nuclei and posterior cingulate regions homologous to rodent RSC is impaired[62]. Subsequent improvements in functional connectivity between the posterior cingulate and prefrontal cortex predict psilocybin-induced enhancements in cognitive flexibility[20]. Importantly, the RSC is involved in the retrieval of remote fear memories, positioning it as a potential substrate for psilocybin's longer-lasting effects[62-66].

To investigate the role of the RSC in the post-acute effects of psilocybin on behavioral flexibility, extinction of trace fear conditioning (TFC) was employed as the appropriate primary behavioral paradigm. TFC is a model of complex fear learning in rodents, in which a conditioned stimulus (CS) is followed by a trace period of 20-seconds preceding the shock. The trace period in TFC renders conditioning and extinction cortex-dependent, requiring protracted attention to associate temporally distant stimuli[68-70]. When the shock is omitted during extinction, animals must learn that it is now safe to reduce their freezing response or extinguish. In mice, Kwapis et al. found that TFC extinction depends on excitatory activity in the RSC[68]. Others have shown that optical, electrolytic, and pharmacological interventions in the RSC impact various kinds and stages of FC[45,49,50,55,63-71]. In a one-day paradigm, psilocybin administered 24 hours prior facilitated TFC extinction at low doses[72]. However, this study did not investigate the effect of psilocybin on long-term, consolidated fear memory, which is of translational interest.

To evaluate the hypothesis that psilocybin promotes behavioral flexibility by rapidly and persistently altering RSC ensembles associated with aversive memories, we investigated the effects of a single dose of psilocybin in a multi-day TFC extinction paradigm. We repeated this experiment in GCaMP8m-expressing, miniature microendoscope-implanted mice to measure single-cell calcium activity throughout the task. Using tensor component analysis (TCA)[73], we identified ensembles driving RSC activity during different cognitive phases of the task - acquisition, early extinction/fear recall, and late extinction. We confirmed our hypothesis that psilocybin accelerates and enhances the recruitment of an extinction-associated ensemble, particularly in drug-responsive animals. To our surprise, we found that fear extinction was also associated with an acute, robust suppression of fear-associated neurons during psilocybin administration. These effects on neural activity predicted extinction, and a computational model revealed that this inhibition is in fact sufficient to explain enhanced recruitment in extinction-associated neurons as well as behavioral variability. Taken together, these results support two mechanisms of psilocybin-enhanced fear extinction in the RSC, based on opposing forms of plasticity, which act in concert to reduce behavioral inflexibility.

Results.

Psilocybin enhances Trace Fear Extinction (TFC) extinction in a responsive subpopulation of mice.

Mice underwent a five-day TFC paradigm, with one Habituation, one Acquisition, and three Extinction Sessions (**Fig. 1a**). Freezing was measured in ezTrack[74] as percent of time immobile during the trace period. Mice were administered psilocybin (1.0 mg/kg, i.p.) or saline 30 min before *Extinction 1*. This time-point

was chosen as psilocybin-induced head twitches, the behavior taken as a proxy for the subjective effects in animals, peak around 15 min and last for up to 150 min[42]. Both groups froze significantly more during the first trace period of Extinction 1 than baseline, indicating successful TFC acquisition (**Supplementary Fig. 1e, Supplementary Table 1**). Psilocybin did not affect recall during Extinction 1, defined as freezing in the first half of the session (**Fig 1b, Supplementary Table 1**). Nonetheless, psilocybin mice reduced freezing more quickly during Extinction 1, indicating that psilocybin acutely accelerated fear extinction. (**Supplementary Fig 1a, Supplementary Table 1**) Psilocybin significantly reduced freezing during early Extinction 2, indicating enhanced extinction recall. By Extinction 3 there was no significant difference between groups, nor at a one-month follow-up (**Fig. 1b, Supplementary Fig. 1a,f, Supplementary Table 1**). Overall, there was no difference between males and females in either condition (**Supplementary Fig. 1b,c, Supplementary Table 1**).

The extinction rate was calculated as the percent difference between freezing in late Acquisition and late Extinction 3. We chose this definition to circumvent the confounding variable of drug-induced changes in mobility during Extinction 1. Notably, there was a trend towards psilocybin-enhanced extinction rate,

with a skewed distribution of extinction rates in psilocybin and saline groups (**Fig. 1c, Supplementary Table 1**). As extinction rate was one of our primary outcomes, mice that had extinguished >50% of their late Acquisition freezing by late Extinction 3 were classified as rapidly extinguishing and all others as slowly extinguishing.

Intriguingly, psilocybin-administered rapidly extinguishing mice reduced freezing more quickly than all other groups (**Fig. 1d, Supplementary Table 1**). This effect was greatest during early Extinction 2, suggesting psilocybin particularly enhanced recall of extinction memory. In contrast, freezing in slowly extinguishing mice was unaffected by treatment (**Fig. 1d, Supplementary Table 1**). There was the same proportion of rapid and slow extinguishing mice in each group (**Fig. 1e**).

To determine whether there was subpopulation of psilocybin non-responsive mice or whether it is always the case that mice that freeze more during recall extinguish slowly, we asked if freezing during the psilocybin's acute effects in Extinction 1 would predict extinction class. (**Fig. 1f,g left, Supplementary Table 1**) Interestingly, the percent freezing during late Extinction 1 predicted classification as either rapidly or slowly extinguishing only if mice were administered psilocybin (auROC = 0.9176, p = 0.0054), but not saline (auROC = 0.6488, p = 0.2225). Indeed, freezing in psilocybin rapid-extinguishers was significantly lower
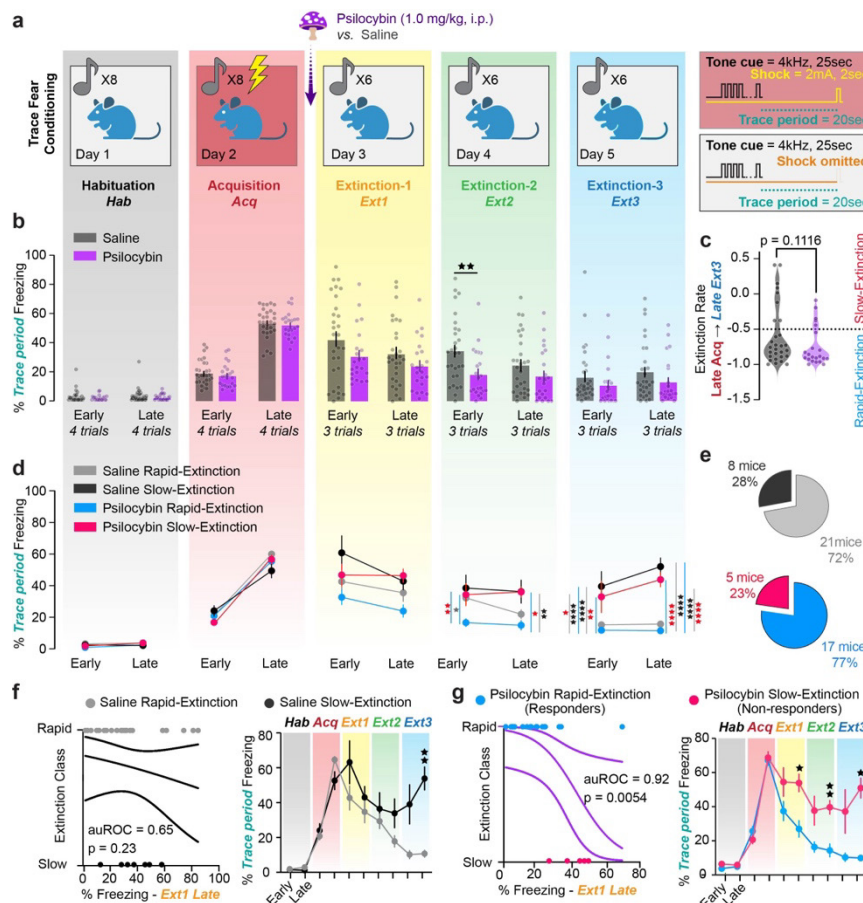
Figure 1 | Psilocybin enhances TFC extinction in a responsive subpopulation of mice.
a. Diagram of five-day TFC experiment. Right-hand panels depict conditioned and unconditioned one parameters. **b.** Average % time freezing during trace period in the first and last 3 trials of each day ("Early," "Late" respectively) in saline and psilocybin-administered mice (black and purple respectively, n=25 each). Dots are individual animals. Two-Way ANOVA with Sidak multiple comparisons correction (Supp. Table 1, rows 1-5) **c.** Extinction rate calculated as the difference between freezing during late Acquisition and late Extinction 3 divided by freezing during late Acquisition. Red line indicates -50% threshold distinguishing rapidly- from slowly-extinguishing mice. Unpaired t-test. (Supp. Table 1, rows 6) **d.** Same as B; treatment groups subdivided into rapid- and slow-extinguishing mice (light colors, rapid; dark colors, slow). Two-Way ANOVA with Sidak multiple comparisons correction. (Supp. Table 1, rows 7-11) **e.** Pie charts describing breakdown of rapid- and slow-extinguishing mice within treatment groups. **f.** Left: Logistic regression predicting extinction rate based on % time freezing during early *Extinction 1* during acute drug treatment in saline-administered mice. Right: Direct comparison of % freezing over time between saline rapid- and slow-extinguishing mice. 2-Way ANOVA. (Supp. Table 1, rows 12-13) **g.** Same as F for psilocybin-administered mice. (Supp. Table 1, rows 14-15) Data are mean ± SEM. * p ≤ 0.05, ** p < 0.01, *** p < 0.001, **** p < 0.0001.

than slow-extinguishers during acute psilocybin administration and consistently throughout the subsequent days. On the other hand, saline rapid- and slow-extinguishers are only differentiated at the timepoints used to define the classes, suggesting there were no pre-existing distinctions between the groups. Thus, we identified two classes of psilocybin-responsive versus non-responsive mice, hereon referred to as "responders" and "non-responders" respectively.

Miniscope-implanted mice acquire and extinguish TFC.

To explore the neurophysiological correlates of psilocybin-enhanced TFC extinction, single cell calcium activity was recorded in the RSC of saline and psilocybin mice. Mice were injected with AAV9-*hSyn*-GCaMP8m in the RSC and two weeks later implanted with a 1.0 mm diameter, gradient refractive index (GRIN) lens over the injection site (**Fig. 2a B**). After 2-5 weeks, mice were trained in the same TFC task (**Fig. 2c**). Calcium traces were extracted using CNMF-E in the Inscopix Data Processing Software API and post-processed (**Fig. 2d**). Across the entire TFC imaging
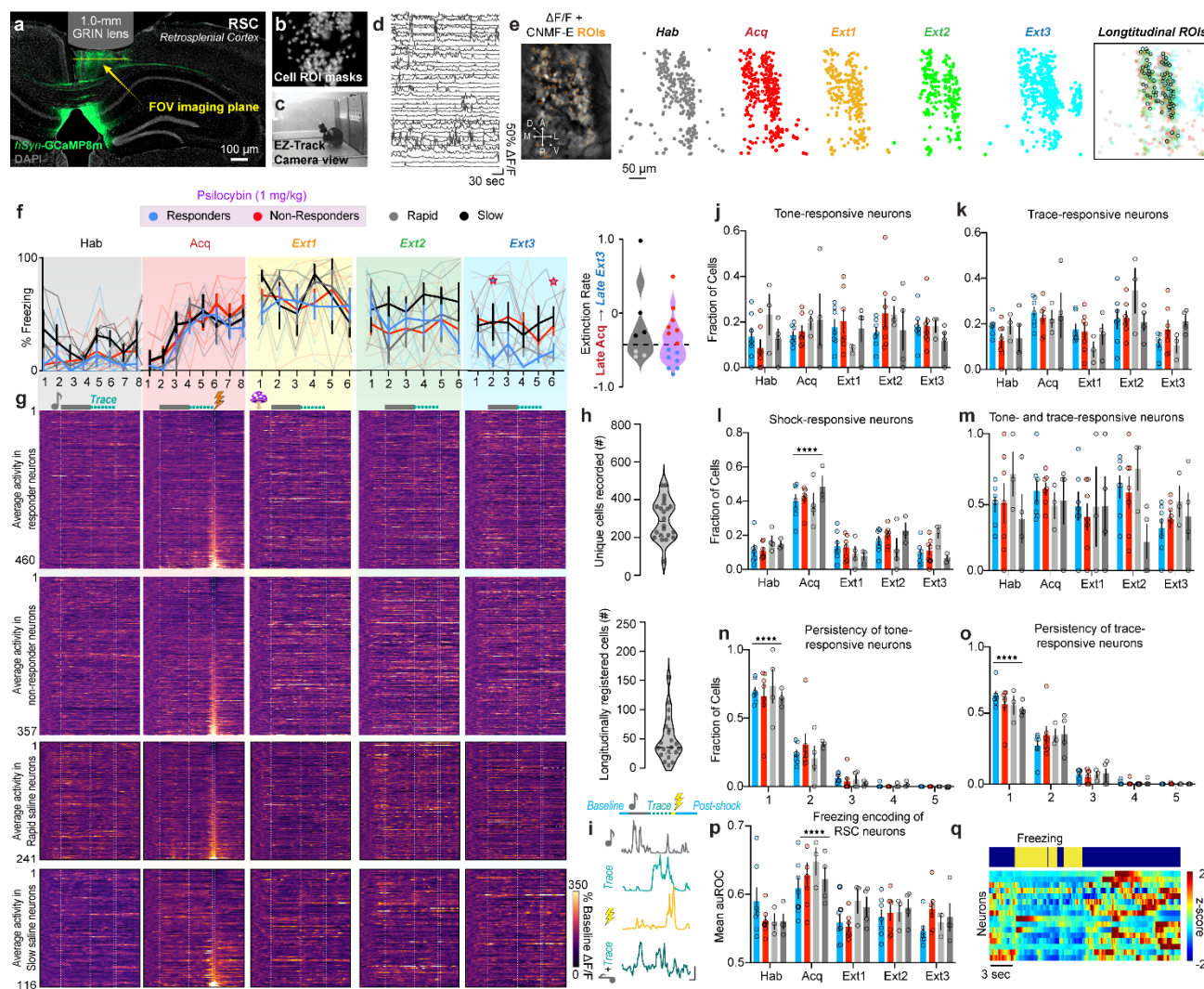
Figure 2 | RSC neurons are modulated over TFC extinction in psilocybin- and saline-administered mice.
a. Representative image of *AAV8-syn-GCaMP8m-WPRE* expression (green) and nuclei (grey) in RSC under GRIN lens tract. **b.** Cell masks of imaged neurons during one session from same mouse. **c.** Image of behavioral set-up during an extinction session. Example frame of freezing mouse. **d.** Example traces of neurons recorded during behavior in dF/F in same mouse. **e.** Left: Representative image from Ca^{2+}-imaging video in the same mouse. Right: Cell masks of each recorded neuron in each session, overlayed with masks of longitudinally registered cells. **f.** Left: Percent of time freezing during each trial in responders (n=7 mice), non-responders (n=7 mice), and saline mice (n=7 mice). Two-Way ANOVA. (Supp. Table 1, rows 16-20) Right: Extinction rate. Unpaired t-test. (Supp. Table 1, row 21). **g.** Average activity in each neuron over all trials from each session, normalized to baseline before one onset and aligned to shock. Top: Responders (n=460 neurons), Top middle: Non-responders (n=357 neurons), Bottom middle: rapid saline (n=241 neurons), Bottom: slow saline (n=116 neurons). **h.** Top: Number of unique cells accepted over all sessions in each animals. Bottom: Number of longitudinally registered neurons in each animal. **i.** Example traces of tone-, trace-, shock-, and tone+trace-responsive neurons (top to bottom). Vertical scale bar = 2dF/F, horizontal scale bar = 5 sec. **j.** Fraction of tone-responsive cells in each group over each day. Two-Way RM ANOVA. (Supp. Table 1, row 22) **k.** Fraction of trace-responsive cells in each group over each day. Two-Way RM ANOVA. (Supp. Table 1, row 23) **L.** Fraction of shock/omission-responsive cells in each group over each day. Two-Way RM ANOVA. (Supp. Table 1, row 24) **m.** Fraction of one-responsive neurons that are also trace-responsive cells in each group over each day. Two-Way RM ANOVA. (Supp. Table 1, row 25) **n.** Fraction of one-responsive cells that are one-responsive for 1-5 days in each animal. Two-Way RM ANOVA. (Supp. Table 1, row 26) **o.** Fraction of trace-responsive cells that are trace-responsive for 1-5 days in each animal. Two-Way RM ANOVA. (Supp. Table 1, row 27) **p.** Average freezing encoding of neurons in each group over each day (auROC, Two-Way ANOVA). (Supp. Table 1, row 28) **q.** Representative traces of freezing-encoding neurons in 1 animal sorted from greatest to least (bottom to top) auROC. Data are represented as mean ± SEM. * p ≤ 0.05, ** p < 0.01, *** p < 0.001, **** p < 0.0001.

protocol, 11-160 RSC neurons per animal (median = 46) were longitudinally registered across all days (Psilocybin responders = 460 total neurons; Psilocybin non-responders = 350 total neurons; Saline rapidly-extinguishing mice = 241 total neurons; Saline slowly-extinguishing mice = 116 neurons total; **Fig. 2e,g,h**). Miniscope placements were validated in all mice (**Supplementary Fig. 2**).

All miniscope mice successfully acquired TFC and were subsequently split into psilocybin (1.0 mg/kg; i.p.; n=14 mice) and saline (n=7 mice; **Fig. 2f left, Supplementary Table 1**). Miniscope implanted mice extinguished less robustly than surgically naïve mice, indicating an impact either of head trauma or chronic stress post-implantation on TFC extinction (**Fig. 2f right, Supplementary Table 1**). Nonetheless, by Extinction 3, a subset of psilocybin responders emerged. Seven of fourteen psilocybin-treated mice and three of seven saline-treated mice extinguished their freezing by over 50% (**Fig. 2f, Supplementary Table 1**).

RSC neurons are modulated over TFC training.

To determine changes in the task-relevant response properties of RSC neurons, fractions of tone-, trace, shock-, and tone+trace-responsive neurons were measured each day (**Fig. 2i**). Fractions of tone- or trace period-upregulated neurons were

not significantly affected over time in any treatment group and in general varied between 10-30% of neurons (**Fig. 2j,k, Supplementary Table 1**). ~40% of recorded RSC neurons were shock-responsive neurons (**Fig. 2l, Supplementary Table 1**). On average, ~50% of tone-responsive neurons on a given day were also trace-responsive on the same day, suggesting a high degree of overlap of activated neurons between different periods in a trial (**Fig. 2m, Supplementary Table 1**). There was a large rate of turnover in tone- and trace-responsive neurons between days, with ~75% of tone- and ~60% trace-responsive neurons maintaining their responsiveness for only 1 day and about ~25% and ~30% respectively for 2 days across groups (**Fig. 2n,o, Supplementary Table 1**).

Similar proportions of all neurons recorded were responsive to various stimuli on each day, indicating that the longitudinally registered neurons subsequently used for analysis comprise a sufficiently representative sample of all recorded neurons. (**Supplementary Fig. 2c-j, Supplementary Table 1**). Within days, the proportion of total shock- and stable tone-and-trace responsive neurons during Extinction 1 positively correlated with freezing in early Extinction 3 in psilocybin mice, and suppressed shock-responsive neurons during Extinction 1 correlated with freezing in early Extinction 3 in saline mice, suggesting that neural response
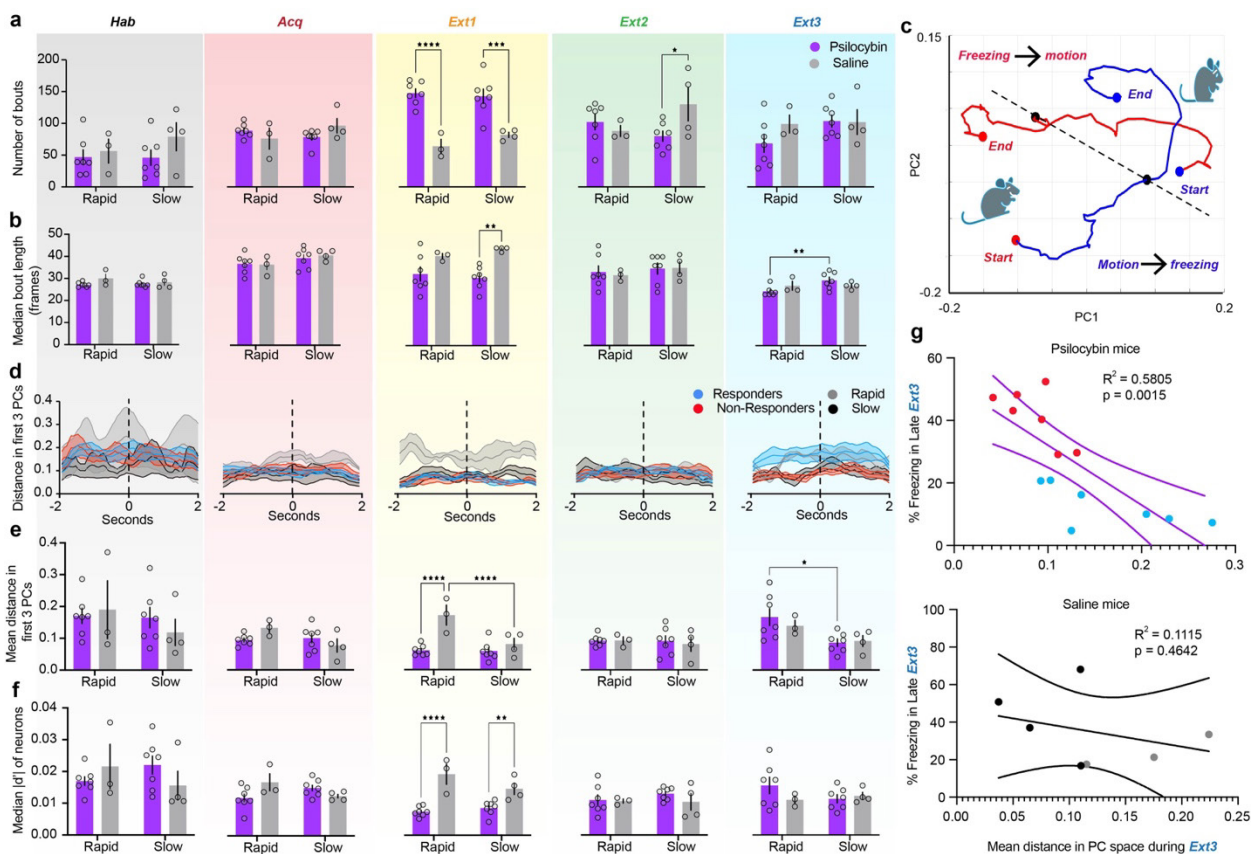
Figure 3 | Psilocybin alters dynamics and encoding of freezing behavior.
a. Total number of freezing bouts per session. (Left to right, Black = Habituation, Red = Acquisition, Yellow = Extinction 1, Green = Extinction 2, Blue = Extinction 3). Two-way ANOVA. (Supp. Table 1, rows 29-33). **b.** Median bout length per session in frames. Two-way ANOVA. (Supp. Table 1, rows 34-38). **c.** Representative average trajectories of motion-to-freezing (blue line, bout start) and freezing-to-motion (red line, bout end) transitions in the first two PCs, from two seconds before to two seconds after transition. (Black point = time of transition, red points = starting and ending points in motion, blue points = starting and ending points in freezing) A dashed line is drawn between the two transition points. **d.** Average Euclidean distance in PC space between each pair of points in motion-to-freezing and freezing-to-motion trajectories in the first three PCs on each day. Dashed line indicates time of behavioral transition. Shaded areas are SEM. **e.** Mean distance in PC space between bout start and bout end over the four-second time window between trajectories. Two-way ANOVA. (Supp. Table 1, rows 39-43). **f.** Median absolute value of d-prime between motion and freezing in all recorded neurons on each day. Two-way ANOVA. (Supp. Table 1, rows 44-48). **g.** Linear regression of distance in PC space between trajectories (Fig. E, right) and % trace period freezing in late Extinction 3 in psilocybin (top) and saline mice (bottom). (Supp. Table 1, rows 49-50). Data are mean ± SEM. * p ≤ 0.05, ** p < 0.01, *** p < 0.001, **** p < 0.0001.

properties during Extinction 1 may be related to behavioral extinction across groups.

Psilocybin alters dynamics and encoding of freezing behavior.

The RSC was host to many neurons encoding freezing behavior in every session (**Supplementary Fig. 2b, Supplementary Table 1**). Interestingly, the average freezing encoding of individual neurons increased during *Acquisition*, suggesting that RSC neurons preferentially encode acute fear-related freezing (**Fig. 2p,q, Supplementary Table 1**). Behaviorally, psilocybin significantly reduced bout number and increased bout length acutely during Extinction 1 without affecting total freezing time, indicating an effect of psilocybin treatment on the ability to maintain sustained freezing (**Fig. 3a,b, Supp Fig. 3, Supplementary Table 1**). This could be due to an interruption of attention to or recall of fear cues.

In non-longitudinally registered neurons, transitions from freezing to motion and vice versa were robustly encoded in the first 3 PCs of RSC activity (**Fig. 3c**). Average Euclidean distance from freezing-to-motion and motion-to-freezing trajectories tended to be stable within this time window. However, distance greater during Extinction 1 in rapidly compared to slowly extinguishing saline mice, a difference occluded by psilocybin (**Fig. 3d, Supplementary Table 1**). Accordingly, single cell discriminability between freezing and motion, in terms of the population's median magnitude of d-prime, was suppressed by psilocybin (**Fig. 3e, Supplementary Table 1**). Interestingly, population freezing was subsequently enhanced in responders during Extinction 3 and predicted freezing levels in psilocybin but not saline mice (**Fig. 3d,f, Supplementary Table 1**). Thus, while RSC discriminability between motion and freezing during Extinction 1 is enhanced in rapidly extinguishing mice, psilocybin acutely suppresses this

Figure 4 | Tensor Component Analysis (TCA) captures evolution of RSC through different task-relevant states over learning. a. Representative rank-5 TCA model of neural activity over RSC in one mouse. Rows correspond to unique components of neural activity and columns correspond to temporal, neuron, and trial factors. Values in each panel correspond to the factor loadings, or weights, of each component at each time, cell, and trial in the given component. Pink dashed line over temporal factors indicates time of conditioned one delivery, and lightning bolt indicates time of shock-delivery. Gradients over the trial factor indicate session of trials (Black = Habituation, Red = Acquisition, Yellow = Extinction 1, Green = Extinction 2, Blue = Extinction 3). Trial weights are color coded according to the animals % time freezing in each trial (dark blue = 0%, bright yellow = 100%). **b.** Normalized trial factor weights for each component, averaged within groups. Two-Way RM ANOVA. (Supp. Table 1, rows 51-55). **c.** Validation of choice of rank-5 model. Left: Four TCA models at each of ranks 1-10 were generated on neurons pooled from all psilocybin administered animals and their reconstruction error (pink) and model similarity (blue) plotted against each other. Rank-5 was chosen by minimizing reconstruction error while maximizing model similarity (black dashed line). (Supp. Table 1, row 56) Right: Reconstruction error (solid colors) and similarity (checkered colors) in individual animals. (Supp. Table 1, row 57) Ordinary One-Way ANOVA with Tukey multiple comparisons correction. **d.** Trial weights of dominant factor during a given session divided by those of each other factor, summed over sessions, calculated over 100 iterations of TCA on real data from each group and TCA models generated on 100 shuffles of the data. Data was shuffled over cells at each individual timepoint to preserve all temporal and trial dynamics of activity that could lead to session discriminability. Multiple unpaired t-tests. P<0.0001 for all comparisons. (Supp. Table 1, row 58) **e.** Linear regression trial factor value of each of 5 components and trial-by-trial freezing across all 5 days (R^2). Significant values are filled and non-significant values are hollow. One-sample t-test. (Supp. Table 1, rows 59-60) **f.** Linear regression of relative strength of each component during each session and extinction rate in all mice (R^2). Numbers are linear coefficients. Stars indicate where slope is significantly non-zero. (Supp. Table 1, row 61-65) **g.** Data in D for the Extinction 3-dominant component during Extinction 3. (Supp. Table 1, rows 66) * p ≤ 0.05, ** p < 0.01, *** p < 0.001, **** p < 0.0001

neural discriminability preceding its rebound 48 hours later in responders. Psilocybin therefore interrupts freezing behavior and encoding in mice.

Tensor component analysis reveals evolution of RSC through different states over fear and extinction learning.

We hypothesized that psilocybin induces the rapid recruitment of a novel Extinction associated ensemble in the RSC during Extinction 1 that persistently drives RSC activity during future extinction sessions. Enhanced extinction could also arise from psilocybin-mediated suppression of specific ensembles associated with the fear learning and memory. To identify ensembles associated with TFC acquisition and extinction, we employed an unsupervised dimensionality reduction technique developed by Williams et al., 2018 called Tensor Component Analysis (TCA) that can be used to group neurons into functional ensembles defined by their within- and across-trial dynamics [73] (**Fig. 4a**).

To determine the appropriate model rank for analysis, TCA was run on cells pooled from all animals in each treatment group to calculate model reconstruction error and similarity as a function of increasing model rank. The elbow method revealed that models of rank 5 were most appropriate for subsequent analysis, and such models were generated for individual animals (**Fig. 4c**) Across animals, rank 5 models did not identify within-trial temporal dynamics beyond shock-responsiveness (**Supplementary**

Fig. 3a-e, Supplementary Table 1). They did, however, cluster trials from the same session, identifying RSC dynamics driving distinct phases of TFC acquisition and extinction (**Fig. 4a,b**).

To eliminate the possibility that trial clustering was due to changes in recording quality between days or cell misalignment, 100 iterations of TCA on the real data from each group were compared to TCA models of 100 shuffles of the neural activity. Neural activity was shuffled by cells at each timepoint, such that the average activity over time and trials was preserved. This way, differences in between- and within-trial temporal dynamics of the entire population would be entirely conserved, but the ensembles driving those differences would be abolished.

To calculate the session discriminability of the real and shuffled TCA models, we exploited the clustering of trial factor weights within a given session, yielding a dominant component for each session. In a model of rank R, for component r in session s with mean trial weights $\bar{w}$, the relative strength of each component. The model's subsequent session discriminability index were calculated as:

$$Strength_{r,s} = \frac{\bar{w}_{r,s}}{\sum_1^R \bar{w}_{r,s}}$$

$$Session\ discriminability = \sum_1 \max(Strength_s)$$
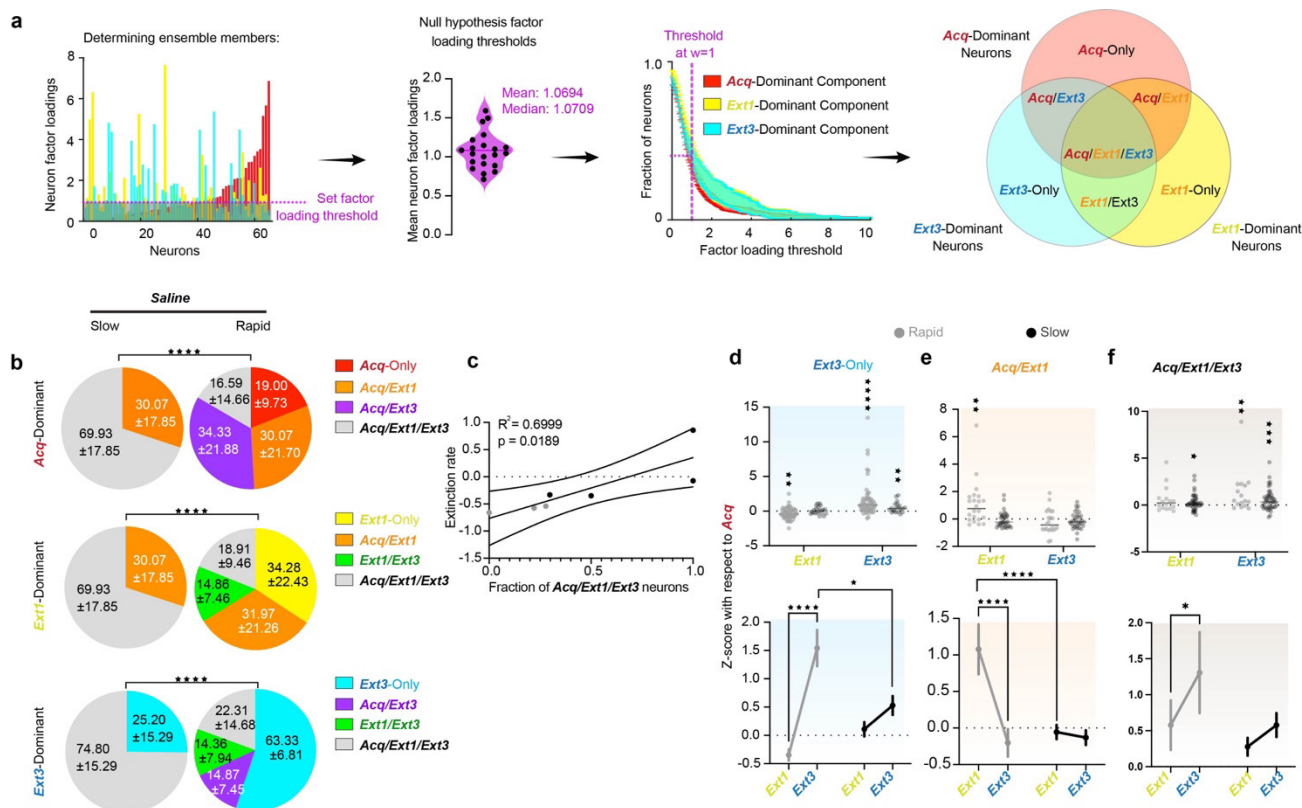
Figure 5 | Turnover in the dominant neural ensembles driving RSC dynamics predicts fear extinction.
a. Choosing Acq-, Ext1-, and Ext3-dominant neurons (red, yellow, and blue, respectively). Left: The fraction of neurons included in the ensemble at various thresholds across animals (mean, SEM) and the neuron factor weights of each neuron in each component in a representative animal. Neurons crossing the chosen threshold of $w=1$ are indicated by enhanced opacity. Middle: Schematic of the overlaps between these neurons, yielding Acq-Only, Acq/Ext1, Ext1-Only, Ext1/Ext3, Ext3-Only, Acq/Ext3, and Acq/Ext1/Ext3. Ensembles are denoted by the corresponding ROYGBIV color code throughout the figure. Right: Example traces. **b.** Pie charts describing the average overlap of the Acq-, Ext1, and Ext3-dominant ensembles (top, middle, bottom) in rapidly and slowly extinguishing saline-administered mice. Numbers are mean ± SEM. Stars indicate comparisons between each psilocybin group and saline. Chi-square test. (Supp. Table 1, rows 67-69). **c.** Linear regression of the fraction of *Acq/Ext1/Ext3* neurons and extinction rate in saline mice. (Supp. Table 1, row 70). **d.** Top: z-score activity in individual *Ext3-only* neurons in each ensemble from Acquisition. Wilcoxon rank-sum to test if change is different from zero. Bottom: Same data displayed as mean ± SEM. Two-way RM ANOVA to compare changes over time and between groups. (Supp. Table 1, rows 71-72). **e,f.** Same as D for *Acq/Ext1* and *Acq/Ext1/Ext3*. (Supp Table 1, rows 73-76). * $p \leq 0.05$, ** $p < 0.01$, *** $p < 0.001$, **** $p < 0.0001$.

When cells were shuffled to preserve the within- and across-trial structure of the data, session discriminability was significantly diminished in every group, rejecting the hypothesis that same-session trial clustering was due to recording or registration artifacts (**Fig. 4d, Supplementary Table 1**). In non-shock control mice, who did not undergo any associative learning beyond neutral sensory integration and context familiarization (*i.e.,* no electric shocks during Day 2 Acquisition), session discriminability was reduced, suggesting TCA identified task-relevant components of RSC activity **(Supplementary Fig. 5a-d, Supplementary Table 1)**.

In conditioned mice, the relative strength of each component strongly also predicted freezing across and within their own session with $R^2 > 0.1$ (**Fig. 4e,f, Supplementary Table 1**). The strength of the *Acquisition*-dominant component during Acquisition and Extinction 3 oppositely predicted freezing, while the *Extinction 3*-dominant component during Extinction 3 strongly predicted extinction rate across groups, suggesting the identification of fear extinction related neural dynamics in the RSC by TCA (**Fig. 4g,**

Supplementary Table 1). These results confirm that the evolution through unique dynamics across days is a learning-related process in the RSC.

Turnover in the dominant neural ensembles driving RSC dynamics predicts fear extinction.

The neuron factor weights returned by TCA were used to identify ensembles driving the *Acquisition*-, *Extinction 1*-, and *Extinction 3*-dominant components of RSC activity in each mouse. When simulated tensors for each animal populated with identically behaving neurons, the mean and median weights were $w = 1.0694$ and 1.0709 respectively, suggesting that, if all neurons contributed equally, each neuron would be assigned $w \sim 1$ (**Supplementary Fig. 6d-g**). Thus, $w=1$ was considered a reasonable null hypothesis for the strength of a neuron's participation in each component, such that if a neuron's weight was greater than 1,
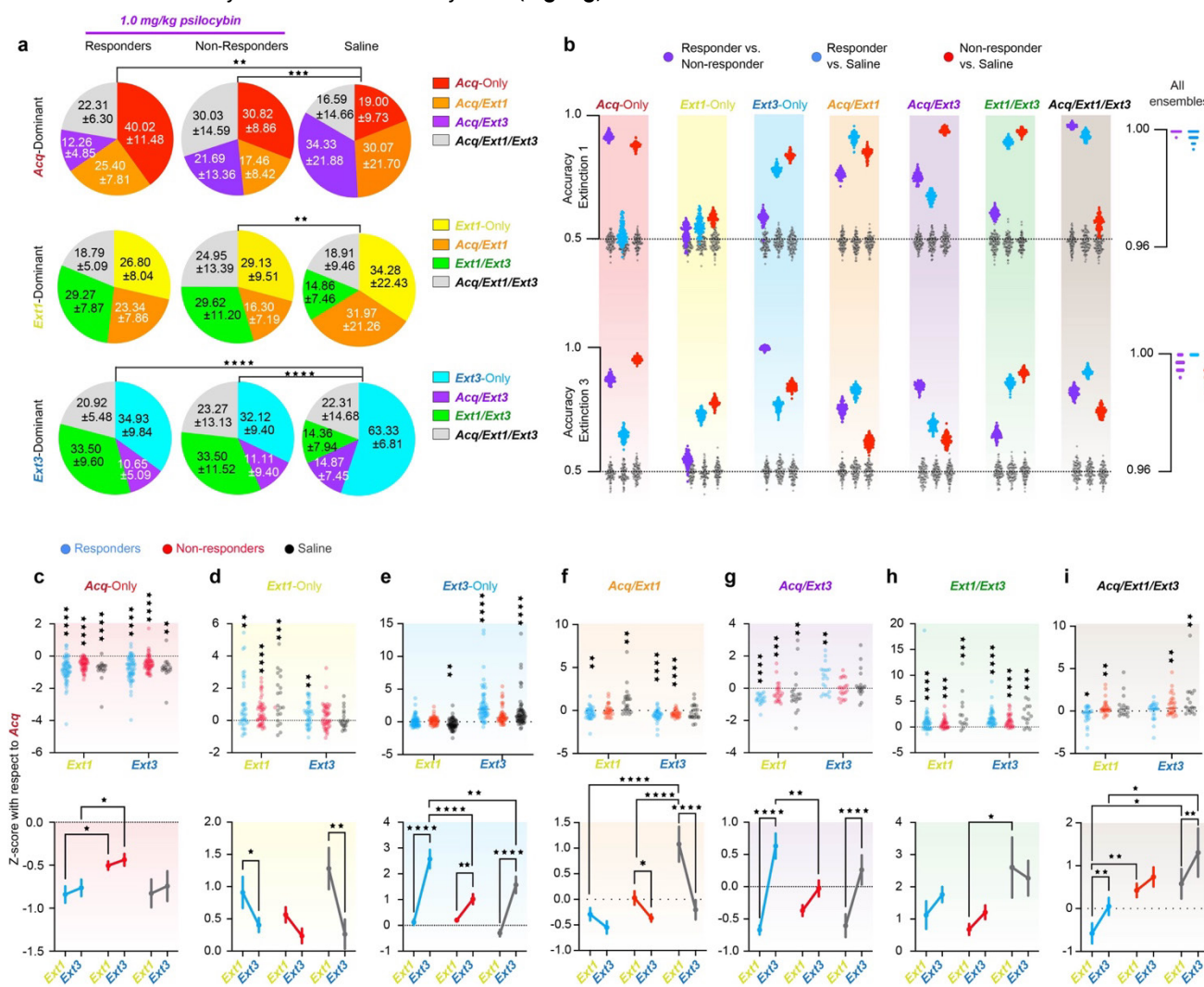
Figure 6 | Psilocybin bidirectionally modulates neural ensembles driving RSC dynamics during TFC in responders.
a. Pie charts describing the average overlap of the Acq-, Ext1, and Ext3-dominant ensembles (top, middle, bottom) in responders, non-responders and rapidly extinguishing saline-administered mice. Numbers are mean ± SEM. Stars indicate comparisons between each psilocybin group and saline. Chi-square test. (Supp. Table 1, rows 77-79) **b.** Accuracies of 100 Fisher decoders trained to predict responder status (left cloud, purple), responders from rapidly extinguishing saline-administered mice (middle cloud, blue around grey), and non-responders from saline administered mice (right cloud, red around grey). Grey clouds are the same decoders tested on shuffled class labels. Decoders were trained on activity during Extinction 1 (top) and Extinction 3 (bottom). Right-hand panels accuracies of decoders trained on all seven ensembles as predictors. **c.** Top: z-score activity in individual Acq-Only neurons in each ensemble from Acquisition. Wilcoxon rank-sum to test if change is different from zero. Bottom: Same data displayed as mean ± SEM. Two-way RM ANOVA to compare changes over time and between groups. (Supp. Table 1, rows 80-81) **d-i.** Same as C for Ext1-Only, Ext3-Only, Acq/Ext1, Ext1/Ext3, Acq/Ext3, and Acq/Ext1/Ext3, respectively. (Supp. Table 1, rows 82-93) * $p \leq 0.05$, ** $p < 0.01$, *** $p < 0.001$, **** $p < 0.0001$

then it was included in the ensemble. 40% of neurons met this criterion for each ensemble, resulting in considerable ensemble overlap (**Fig. 5a,b, 6a, Supplementary Fig. 4a-c, Supplementary Table 1**). Ensemble overlaps are of interest as cells driving RSC dynamics on both *Acquisition* and *Extinction 1*, for instance, might in part comprise a neural substrate for a fear memory[61].

Intriguingly, although every combination of these ensembles (*Acq-Only, Ext1-Only, Ext3-Only, Acq/Ext1, Acq/Ext3, Ext1/Ext3, and Acq/Ext1/Ext3*) were represented rapid saline mice, slow saline mice failed to recruit any new dominant neurons in Extinction 1, resulting in a large *Acq/Ext1/Ext3* ensemble and smaller *Acq/Ext1* and *Ext3-only* ensembles (**Fig. 5b, Supplementary Table 1**). Rapidly extinguishing mice recruited a new Extinction 1-dominant ensemble and suppressed a portion of the Acquisition dominant ensemble (19%, *Acq-only* neurons). However, slowly extinguishing mice did neither until Extinction 3, where only 25% of neurons were recruited compared to 55% in rapidly extinguishing mice. The proportion of *Acq/Ext1/Ext3* neurons strongly predicted extinction rate in saline mice, confirming the interpretation that ensemble turnover is associated with effective fear extinction (**Fig. 5c, Supplementary Table 1**).

Tracking the change in activity in these ensembles from Acquisition revealed that slowly extinguishing mice display blunted plasticity in the *Ext3-only* and *Acq/Ext1* neurons compared to rapidly extinguishing mice (**Fig. 5d,e, Supplementary Table 1**). While *Acq/Ext1/Ext3* neurons are significantly more activated during Extinction 1 and Extinction 3, rapid mice display a strong enhancement of *Acq/Ext1* and *Ext3-only* activity during Extinction 1 and 3 respectively, while *Acq/Ext1* neurons are maintained, and *Ext3-only* neurons weakly enhanced in slowly extinguishing mice. Instead, an enhancement *Acq/Ext1/Ext3* activity appears to be the defining feature of RSC activity in slow-extinguishing mice (**Fig. 5f, Supplementary Table 1**). Thus, both in terms of neuronal identity and activation, plasticity in dominant RSC ensembles appears to be a feature of effective TFC extinction.

Psilocybin enhances extinction-associated ensemble turnover.

Both responders and non-responders exhibited high ensemble turnover, in contrast to slowly extinguishing saline mice. To investigate the effect of psilocybin on plasticity of RSC ensembles, responders and non-responders are compared only to rapid saline mice, due to the nonexistence of these ensembles in slowly extinguishing mice. Ensemble overlaps significantly differed between psilocybin and rapid saline mice in most cases, but not between responders and non-responders (**Fig. 6a top, Supplementary Table 1**). The overlap between *Acq-* and *Ext1-*dominant neurons was similar across all groups. Non-responders exhibited the greatest proportion of *Acq/Ext1/Ext3* neurons, while rapid saline mice exhibited the greatest proportions of *Acq/Ext1* and *Acq/Ext3* neurons. Responders displayed the greatest proportion of *Acq-only* neurons, the only ensemble defined by its persistent suppression during both Extinction 1 and Extinction 3. Though only a greater proportion of the *Ext1-*dominant ensemble is defined by newly recruited neurons in psilocybin mice than in rapid saline mice, (**Fig. 6a middle**). Psilocybin mice recruited double proportion of *Ext1/Ext3* neurons. Finally, while more neurons were newly recruited in the *Ext3-*dominant ensemble in rapid saline mice, similar proportions of neurons had been recruited after Acquisition (**Fig. 6a bottom, Supplementary Table 1**). The proportion of *Ext1/Ext3* neurons comprising the Extinction 3-dominant ensemble was triple that of saline mice in psilocybin mice. Thus, psilocybin acutely accelerates a rapid turnover from fear

Acquisition-dominating neurons to a stable Extinction-dominant population. This result is highly consistent with the hypothesis that psilocybin both establishes and stabilizes novel neural ensembles. In non-shock controls, the proportion of *Acq/Ext1* and *Acq/Ext1/Ext3* neurons was much smaller than in saline mice, while there were more *Ext1/Ext3* neurons. (**Supplementary Fig. 5e-g, Supplementary Table 1**). These result supports the hypothesis that preferential overlaps of *Acq/Ext1-* and *Ext1/Ext3-*dominant ensembles, in saline and psilocybin mice respectively, indicate enhanced stability of fear acquisition- and extinction-related ensembles over time.
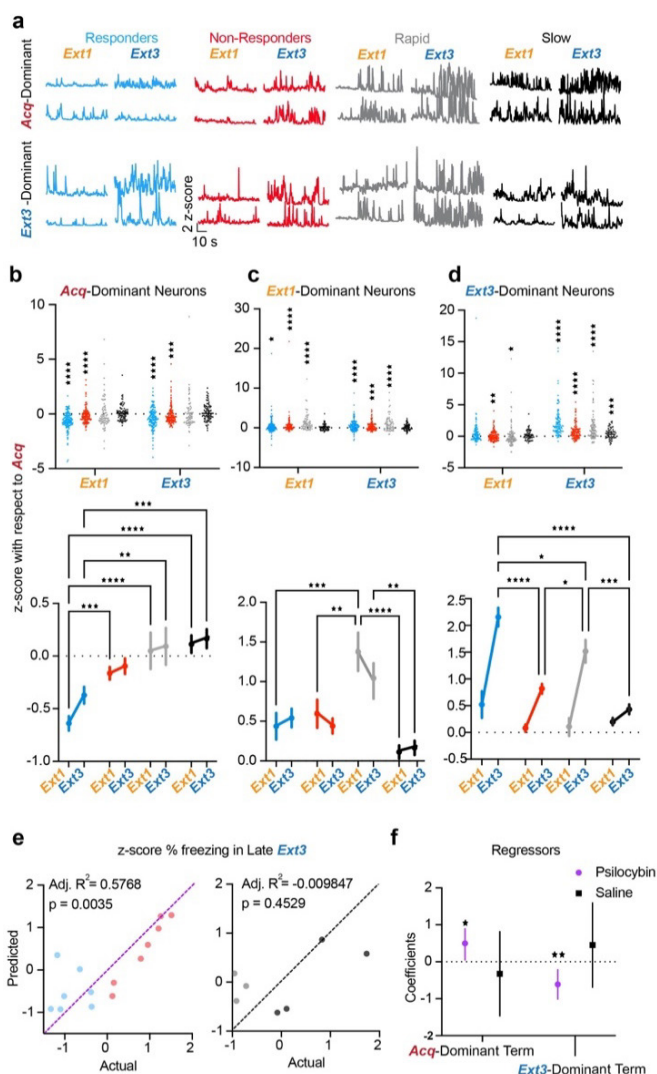
Figure 6 | Psilocybin induces long-term suppression of Acq-dominant neurons and strong post-acute recruitment of Ext3-dominant neurons in responders.

a. Example traces of Acq-dominant (top) and Ext3-dominant (bottom) neurons during Extinction 1, and Extinction 3 in each group. **b.** Top: z-score with respect to Acquisition of individual Acq-dominant neurons in each ensemble during Extinction 1 and 3. Wilcoxon rank-sum to test if median ≠ 0. Bottom: Same data displayed as mean ± SEM. Two-way RM ANOVA to compare changes over time and between groups. Data are represented as mean ± SEM. (Supp. Table 1, rows 94-95) **c.** Same as B) for Ext1-dominant neurons. (Supp. Table 1, rows 96-97) **d.** Same as B) for Ext3-dominant neurons. (Supp. Table 1, rows 98-99) **e.** Multiple regression of z-score % freezing in late Extinction 3 on z-score from Acquisition of activity of *Acq*-dominant neurons in Extinction 1 and *Ext3*-dominant neurons in Extinction 3 in psilocybin (left) and saline mice (right). (Supp. Table 1, rows 100-1) **f.** Mean ± 95% confidence intervals of regression coefficients. (Supp. Table 1, row 102) * $p \leq 0.05$, ** $p < 0.01$, *** $p < 0.001$, **** $p < 0.0001$

Activity in neural ensembles predicts treatment and responder status.

Fisher linear decoders were trained to distinguish between psilocybin responders, non-responders, or saline mice based on the average activities of each identified ensemble during either *Extinction 1* or *Extinction 3* (**Fig. 6b, Supplementary Fig. 4d-e**). Decoders were trained to classify two groups at a time – responders vs. non-responders, responders vs. saline, non-responders vs. saline to determine which ensembles varied with treatment, extinction class, or both.

During Extinction 1, when psilocybin mice were under acute influence of the drug, the *Ext3-Only* and *Ext1/Ext3* ensembles specifically distinguished both groups of psilocybin mice from saline mice, suggesting that psilocybin affected activity in these ensembles in a behavior-nonspecific fashion (**Fig. 6b top**). The *Acq/Ext1* and *Acq/Ext3* ensembles discriminated between all groups, suggesting that psilocybin's acute effects on these neurons can predict future behavioral change. The *Acq/Ext1/Ext3* ensemble only discriminated between responders and the other two groups, suggesting that, while this ensemble is not determinately affected by psilocybin, altered activity in this ensemble during psilocybin administration may enhance future behavioral change. The *Acq-Only* ensemble significantly distinguished non-responders from the other two groups, suggesting that altered activity in this ensemble under psilocybin may block future behavioral change. During *Extinction 3*, the *Ext3-Only* ensemble came to distinguish all three groups (**Fig. 6b bottom**). These results suggest that psilocybin acutely alters dynamics in these neurons acutely and post-acutely in a manner predicting behavior.

When models were trained on all seven ensembles as predictors, they predicted treatment and responder status with > 95% accuracy on all 100 iterations for each pair (**Fig. 6b right**). Classification between all three groups verified these results (**Supplementary Fig. 4e-f**). The ability of many ensembles to distinguish responder status during Extinction 1 suggests that neural activity in the RSC during psilocybin exposure may be a crucial determinant of therapeutic-like response 48 hours later.

Acute suppression of *Acq*-dominant neurons and delayed recruitment of *Ext3*-dominant neurons predict psilocybin-enhanced extinction.

To explore the development of the distinctive predictive characteristics of each ensemble, we calculated how the activity of each neuron in these ensembles changed from the Acquisition session. *Acq-Only* neurons were suppressed during Extinction 1 and Extinction 3 in all groups, but significantly less so in non-responders, suggesting that the suppression of this ensemble during early extinction may affect the pace of fear extinction in mice (**Fig. 6c, Supplementary Table 1**). *Ext1-Only* neurons were potentiated in all groups during Extinction 1, but only remained significantly greater than zero during Extinction 3 in responders (**Fig. 6d, Supplementary Table 1**).

However, this ensemble had limited predictive abilities regarding both responsiveness and treatment, weakening the claim that this difference is crucial for psilocybin's effects on TFC extinction. *Ext3-Only* neurons were strongly recruited in all groups in Extinction 3, but significantly more greatly in responders, suggesting that this enhanced activation of *Ext3-Only* neurons 48 hours after drug administration may drive enhanced TFC extinction in responders (**Fig. 6e, Supplementary Table 1**).

Acq/Ext1 neurons were significantly suppressed during Extinction 1 in responders, unchanged in non-responders, and enhanced in rapidly extinguishing mice, underlying this ensembles' ability to distinguish between all three groups (**Fig. 6f, Supplementary Table 1**). This result suggests that, although psilocybin results in the suppression of *Acq/Ext1* neurons 48 hours after drug administration in both responders and non-responders, it may only ultimately enhance extinction when *Acq/Ext1*-dominant neurons are suppressed during acute drug effects. The *Acq/Ext3*-dominant ensemble was significantly suppressed in Extinction 1 in all animals, and subsequently strongly potentiated with respect to Acquisition levels in Extinction 3 in responders and rapid saline mice, suggesting that these neurons were suppressed during acute drug effects and subsequently re-recruited in responders (**Fig. 6g, Supplementary Table 1**). Likewise, the *Ext1/Ext3*-dominant ensemble was potentiated across days with respect to Acquisition in all groups, but most greatly in rapid saline mice, potentially compensating for its reduced numbers in saline mice (**Fig. 6h, Supplementary Table 1**). Finally, the *Acq/Ext1/Ext3* ensemble driving activity in all three sessions was suppressed during Extinction 1 in responders but potentiated in non-responders and saline mice (**Fig. 6i, Supplementary Table 1**). This result suggests that acute suppression of this ensemble during psilocybin administration may enhance the likelihood of enhanced TFC extinction.

For a holistic picture of these results, one can consider the entire *Acq*-, *Ext1*-, and *Ext3*-dominant ensembles. In saline mice, the *Acq*-dominant ensemble is persistently active at Acquisition-like levels throughout Extinction, regardless of extinction rate (**Fig. 7b, Supplementary Table 1**). This result is specific to TFC-trained mice, as opposed to non-shock mice, indicating the persistence of a potential substrate for fear memory throughout extinction in saline mice (**Supplementary Fig. 5h, Supplementary Table 1**). In contrast, psilocybin persistently suppresses the *Acq*-dominant ensemble, strongly in responders and weakly in non-responders (**Fig. 7b, Supplementary Table 1**). The *Ext1*-dominant ensemble is potentiated throughout extinction in all groups, though most in rapid mice due to the lack of inhibition of overlapping *Acq*-dominant neurons, unlike psilocybin mice, and the presence of newly recruited neurons, unlike slowly extinguishing mice (**Fig. 7c, Supplementary Table 1**). Finally, recruitment of the *Ext3*-dominant ensemble more greatly in saline mice than non-shock controls, suggesting that heightened activity in novel RSC ensembles is a feature of TFC extinction (**Fig. 7d, Supplementary Table 1**). However, the *Ext3*-dominant ensemble is most greatly recruited in both responders and rapidly extinguishing saline mice, suggesting that this recruitment is a fixed feature of effective fear extinction in the RSC, regardless of treatment. However, its recruitment was enhanced in psilocybin responders compared to rapid saline mice. Critically, these results were robust to varying the factor loading thresholds determining a neuron's ensemble membership (**Supplementary Fig. 6a-c, h**).

To determine the relationship between changes in neural activity and behavior, we regressed percent time freezing in the last half of Extinction 3 on the change in neural activity of the *Acq*-dominant ensemble during Extinction 1 and the *Ext3*-dominant ensemble of Extinction 3. (**Fig. 7e,f**) We found that these variables both significantly and oppositely predicted freezing in psilocybin mice but not saline mice. Thus, psilocybin may enhance TFC extinction in animals by bidirectionally modulating ensembles underlying distinct phases of TFC.

A computational model of a two-ensemble RSC microcircuit explains psilocybin's effects.

Acq-dominant neurons are largely shock-responsive (**Fig. 8a**). Ideally, to test their causal influence on psilocybin-enhanced extinction, we would capture and manipulate this functional ensemble, with methods such as TRAP or scFlare paired with opto- or chemogenetics. These approaches require that the targeted

neurons have largely homogenous and stable response properties, distinct from the general population, across trials. However, we found that most neurons significantly respond to the shock on only 1-3 of the total 8 trials (**Supplementary Fig. 7a,d**). Importantly, on each trial, the set of shock-responsive neurons only overlaps by 30-40% with any other trial (**Supplementary Fig. 7b**), while a similar proportion of the general population are also shock responsive (**Supplementary Fig. 7c**). Thus, this functional population does not meet the criteria necessary for these techniques, as
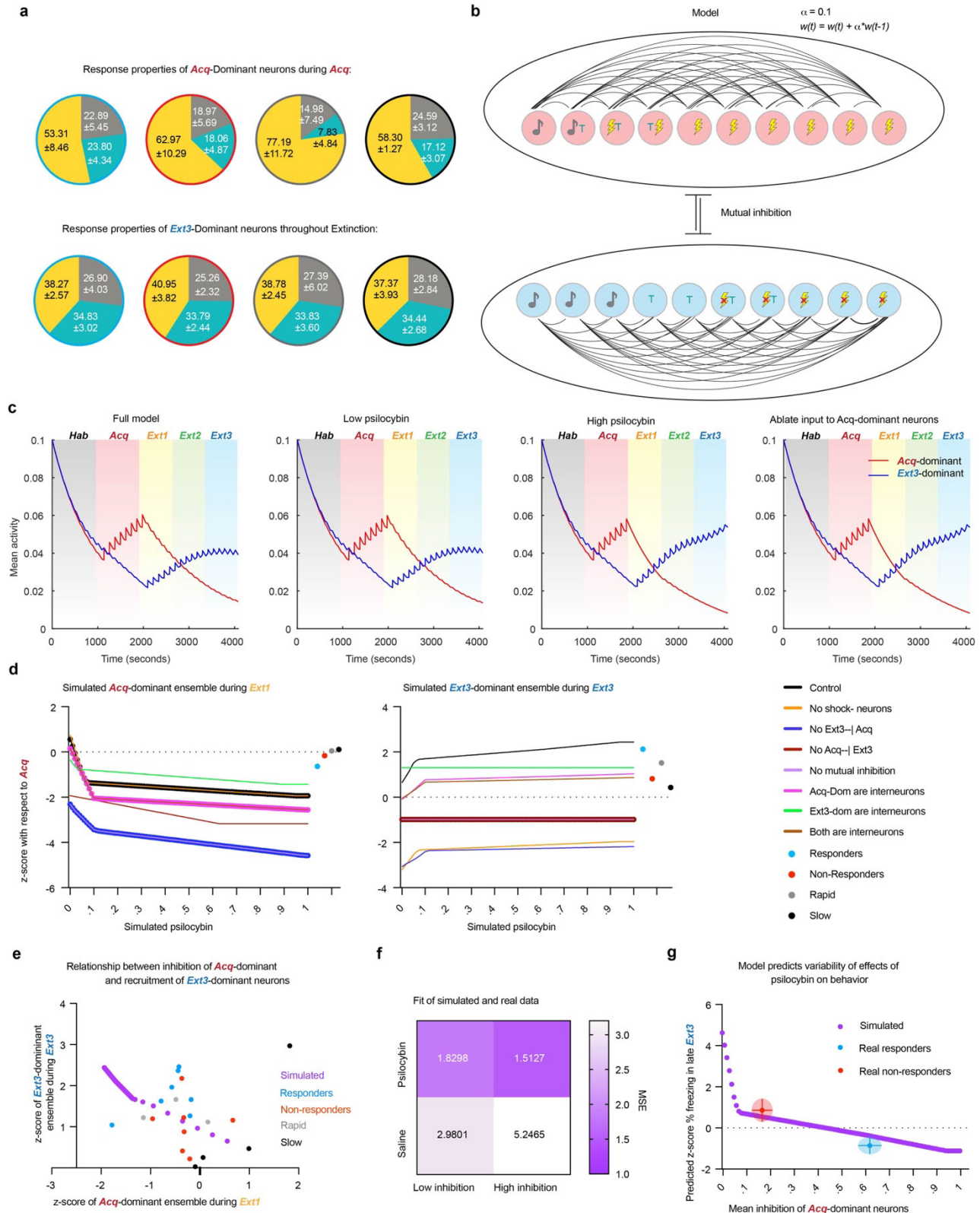
Figure 8 | *Legend continued next page.*

TRAP or scFlare tagging would be nonspecific and insensitive to *Acq*-dominant neurons with trial-varying response properties.

Therefore, to determine whether inhibition of the *Acq*-dominant ensemble by psilocybin could be sufficient to explain either enhanced recruitment of the *Ext3*-dominant ensemble and/or behavioral variability in extinction, we built a linear-nonlinear firing rate model of a hypothesized RSC microcircuit. Each of the two ensembles was modeled with ten recurrently connected units undergoing Hebbian plasticity, with heterogeneous response properties mimicking the real data. These included eight shock responsive units in the *Acq*-dominant ensemble and five shock omission-responsive units in the *Ext3*-dominant ensemble (**Fig. 8a,b**). Crucially, each ensemble inhibited the other. Psilocybin was simulated as varying amounts of direct synaptic inhibition ranging between 0 and 1.

The average activity of the *Acq*-dominant units spiked during each shock-delivery and increased over Acquisition (**Fig. 8c**). Under no and low amounts of psilocybin inhibition, *Acq*-dominant units also spiked during the first trial of Extinction 1 before gradually reducing their activity over time, demonstrating successful modeling of fear conditioning (**Fig. 8c, panels 1 & 2**). Subsequently, the shock-omission-sensitive *Ext3*-dominant ensemble elevated its activity over Extinction. This result demonstrates that the recruitment of *Ext3*-dominant neurons over extinction is a feature of this mutually inhibitory circuit, as our data suggest.

At the highest dose of inhibition and in the positive control case of entirely ablating inputs to the *Acq*-dominant ensemble, the conditioned response of the *Acq*-dominant ensemble during Extinction 1 is eliminated and activity of the *Ext3*-dominant ensemble is enhanced in Extinction 3 (**Fig. 8c, panels 3 & 4**). Therefore, inhibition of *Acq*-dominant ensembles is sufficient to explain enhanced recruitment of *Ext3*-dominant neurons.

To determine whether the assumptions in this model are necessary for its validity, we assessed the activity changes of the ensemble while systematically varying underlying assumptions about the circuit's architecture (**Fig. 8d**). Importantly, for the model to be valid, the case of no inhibition must account for saline mice who undergo recruitment of *Ext3*-dominant ensemble without inhibition of the *Acq*-dominant. This criterion rules out every case other than our full model, where *Acq*- and *Ext3*-dominant ensembles are defined as excitatory populations that mutually inhibit one another.

To determine how well our full model explains our results, we plotted the activity of the *Ext3*-dominant ensemble during Extinction 3 as a function of that of the *Acq*-dominant ensemble during Extinction 1 alongside the average values of each mouse (**Fig. 8e**). The model predicts that there is a nonlinear relationship between inhibition of *Acq*-dominant neurons and recruitment of *Ext3*-dominant neurons, comprised of a shallow quasi-linear part ranging over lower inhibition and a steep quasi-linear part ranging over greater inhibition. To determine which part fits psilocybin or saline data, we calculated the slopes of these lines and the mean squared error (MSE) to our real data (**Fig. 8f**) We found that while both parts strongly fit the psilocybin data, they more weakly fit the saline data, as expected. Compellingly, while the high inhibition part fit the psilocybin data best (MSE$_{high\ inhibition}$ = 1.5127, MSE$_{low\ inhibition}$ = 1.8298), the low inhibition part fit the saline mice better (MSE$_{high\ inhibition}$ = 5.2465, MSE$_{low\ inhibition}$ = 2.9801). These results are consistent with our observations that 1) inhibition of *Acq*-dominant ensembles is only partially present in rapid mice, while it is a consistent phenomenon in psilocybin mice (**Fig. 6c-i**) and 2) degree of inhibition of *Acq*-dominant neurons is only related to degree of subsequent recruitment of *Ext3*-dominant neurons in psilocybin mice (**Fig. 7b-d**).

Finally, to determine whether the model explains the distribution of behavioral variability of freezing in late Extinction 3, we calculated the simulated z-score % freezing using the multiple regression model from Fig. 7e,f (**Fig. 8g**). Indeed, we found that the steep, high inhibition part of the model explains the reduction of freezing in responders as a function of mean inhibition of the *Acq*-dominant ensemble and the failure do so in non-responders, with the predicted freezing lying within a standard deviation of the mean values for each group.

Discussion.

In this study, we combined *in*-vivo single cell calcium imaging of cortical ensembles with behavioral pharmacology to elucidate the neural correlates of psilocybin-enhanced extinction. The existence psilocybin-responsive and non-responsive subpopulations of humans and rats has been the subject of recent investigation[28,75]. Here, we report for the first time that mice are divided into psilocybin responsive and non-responsive groups with respect to post-acute enhancement of TFC extinction. In drug-responsive animals, psilocybin enhances expression of extinction 24 and 48 hours later. In non-responsive animals, psilocybin has no effect on behavior compared to extinction rate-matched saline animals. Acutely, psilocybin increased freezing bouts while decreasing freezing length, suggesting an acute disruption of attention or recall processes. In miniscope-implanted mice, these behavioral changes were accompanied by a reduction of single cell and population-level discriminability between freezing and motion, raising the intriguing possibility that psilocybin could acutely impair the perception of self-motion. Freezing-encoding then recovered

---

Figure 8 *continued* │ A computational model of a two-ensemble RSC microcircuit explains psilocybin's effects.
a. Fractions of tone, trace, and shock responsive neurons in the *Acq*-dominant ensemble during Acquisition (top) and *Ext3*-dominant neurons over all extinction sessions. **b.** Diagram of computational model of *Acq*- and *Ext3*-dominant ensembles and learning function. **c.** Average activity of ensembles over each simulation of the full model with no simulated psilocybin (first panel), low psilocybin simulated as direct synaptic inhibition to *Acq*-dominant units (second panel) during Extinction 1, high psilocybin during Extinction 1 (third panel), and with all synaptic input to the *Acq*-dominant units ablated during during Extinction 1 (last panel). **d.** Z-score with respect to Acquisition of *Acq*-dominant neurons during Extinction 1 (left) and of *Ext3*-dominant neurons during Extinction 3 (right) over multiple conditions: the full model (black), without shock-omission sensitive neurons (yellow), without inhibition of *Acq*-dominant units by *Ext3*-dominant units (deep blue), without inhibition of *Ext3*-dominant units by *Acq*-dominant units (deep red), without mutual inhibition (purple), if *Acq*-dominant units were inhibitory interneurons (pink), if *Ext3*-dominant units were inhibitory interneurons (green), if all units were inhibitory interneurons (brown). Mean values of real data are plotted to the right of each plot. **e.** Real and simulated z-score with respect to Acquisition of *Ext3*-dominant neurons during Extinction 3 plotted as a function of *Acq*-dominant neurons during Extinction 1. Simulated data (purple), responders (blue), non-responders (red), rapid mice (gray), and slow mice (black). **f.** Mean squared error (MSE) of the real data (rows) from the simulated data (columns) in E. **g.** Simulated z-score freezing late Ext3 in model as a function of amount of synaptic inhibition (purple). Average freezing and average inhibition of *Acq*-dominant neurons in responders (blue) and non-responders (red). Error bars and clouds are SD.

in Extinction 3 and predicted freezing in psilocybin mice, suggesting that recovery of freezing encoding is a biomarker of effective psilocybin-modulated fear extinction.

We used TCA to identify trial-varying components of neural activity associated with fear extinction and putative task-relevant ensembles[73]. Consistent with the hypothesis that the RSC preferentially encodes the cognitive or behavioral context associated as opposed to explicit sensory events, the trial factor weights of these components tended to cluster trials from the same session without clear organization of the temporal factor weights across animals, a characteristic significantly reduced in non-shock controls. As the RSC is also involved in contextual fear conditioning and may therefore exhibit similar neural correlates in both paired and unpaired conditioning protocols, non-shock controls isolate fear acquisition- and extinction-related signals from those associated with neutral contextual novelty, exploration, and integration[39-71].

The RSC generates, hosts, and updates engrams for consolidated fear and extinction memory. For instance, freezing can be evoked in a novel context by optogenetically reactivating RSC-tagged neurons that were initially active during fear learning in another context (*i.e.,* akin to the Acquisition session responsive cells)[51,56]. In the present study, candidate neurons for engrams related to fear recall and extinction should be comprised of overlaps between the *Acq-*, *Ext1-*, and *Ext3-*dominant ensembles, such that a subset of *Acq/Ext1* and *Acq/Ext1/Ext3* ensembles participates in a fear engram, while a subset of *Ext1/Ext3* or *Ext3-only* neurons comprise an extinction engram. The behavioral relevance of these ensembles is demonstrated by accurate decoding between responders, non-responders, and rapid saline-treated mice based on each ensemble's activity.

Consistent with previous findings and as the RSC is necessary for TFC, we found a high proportion of overlapping *Acq/Ext1* and *Acq/Ext1/Ext3* neurons in saline mice[61]. Intriguingly, psilocybin reduced this proportion, while the dominant ensembles in slow saline mice were solely comprised of these neurons. The predominance of these ensembles at the expense of *Acq-only, Ext1-only,* and *Ext1/Ext3* neurons in slowly extinguishing saline mice, and the predictive power of the proportion of *Acq/Ext1/Ext3* neurons over extinction rate in saline mice, support the interpretation that the maintenance of fear experience-dominating neurons maintains fear-related behavior. The reduction in putative "fear memory" neurons in psilocybin mice resulted in a doubling of *Acq-Only* neurons, suggesting that psilocybin induced a robust turnover in the composition of the ensembles driving RSC activity in the Extinction 1 session. Finally, a greater proportion of *Ext1/Ext3* neurons were observed in psilocybin than saline mice, suggesting that the ensembles recruited under psilocybin were more stable in the days to come. This observation agrees with dendritic and synaptic plasticity studies that demonstrate psilocybin rapidly induces the formation and subsequent long-term stabilization of behaviorally relevant neural pathways. However, the lack of association between size of these ensembles with extinction rate ruled out the possibility that ensemble turnover alone influences psilocybin responsiveness.

Previous work showed that that novel ensembles are recruited in the RSC during fear extinction[56]. Indeed, we observed a substantial recruitment of neurons unique to the *Ext3-*dominant ensemble in all groups, with significantly lesser activation in non-shock mice. These neurons were significantly more strongly activated during Extinction 3 in psilocybin responders than in any other group. However, this recruitment was preceded by the acute and robust inhibition of *Acq-*dominant neurons in psilocybin

responders that was strikingly absent in saline mice. We found that both the overall inhibition of the *Acq-*dominant ensemble during psilocybin administration and the subsequent recruitment of *Ext3-*dominant neurons during Extinction 3 strongly predicted freezing in late Extinction 3 in psilocybin mice, but not saline mice. Furthermore, by modeling these ensembles as mutually inhibitory populations comprised of excitatory neurons, we not only replicated the neural dynamics observed in saline mice but demonstrated that varying the acute inhibition of *Acq-*dominant neurons during Extinction 1 is sufficient for enhanced recruitment of the *Ext3-*ensemble and extinction in principle.

All other versions of the model where the underlying assumptions of circuit architecture were altered failed to explain the recruitment of *Ext3-*dominant neurons in the absence of *Acq-*dominant inhibition observed in saline mice. Therefore, we can conclude that 1) *Acq-* and *Ext3-*dominant ensembles are likely polysynaptically, mutually inhibitory excitatory populations in the RSC and 2) the inhibition of *Acq-*dominant neurons is sufficient to explain neural and behavioral variability in our task in response to psilocybin. Given all mice received the same dose of psilocybin, these results raise the exciting possibility that individual differences in receptor availability or circuit anatomy in the RSC facilitate psilocybin-enhanced fear extinction.

These results complicate the prevailing hypotheses in the field that psilocybin's effects on behavioral flexibility are downstream of excitatory activity and plasticity enacted via 5HT2ARs[8]. To the contrary, we observed no increased activity under acute psilocybin. As the RSC is rich in 5HT2CRs and 5HT1Ars, both inhibitory with high binding affinity to psilocin, it is plausible that psilocin directly inhibits neurons in this region[28,60,61,76]. Alternatively, psilocin could excite inhibitory neurons upstream of *Acq-*dominant neurons to exert its effects. Therefore, it is possible that behavioral variability under psilocybin in this task could be due to variability in receptor expression and availability or in anatomical connectivity.

Identifying these neurons will be key to establishing their causal influence on fear extinction with or without psilocybin and potentially developing targeted therapeutics. One possibility is that these neurons are salience or valence-sensitive. Notably, a single-dose of psilocin reduces neural activities to aversive airpuffs in the central amygdala days later, hinting that weakened neural activities within negative valence-encoding circuits may partially contribute to this observation[77]. In the RSC, our data and model suggest that *Acq-* and *Ext3-*dominant ensembles contain neurons responsive to shock or shock omission, stimuli of opposite valence. Furthermore, our observations echo the finding that inhibitory plasticity in hippocampus fear memory engrams is necessary for the development memory selectivity, measured by the reduction of freezing in neutral contexts over time[78]. As RSC neurons can encode changes in reward values[47,48], ensembles in this study could constitute a valence- or salience-sensitive ensembles in the RSC, a feature that can enable their genetic and anatomical identification. Taken together, these results suggest that psilocybin both enhances endogenous mechanisms of fear extinction – the potentiation of newly recruited RSC neurons – and, or possibly because, it engages non-typical mechanisms as well – the suppression of fear acquisition-dominating neurons in drug responders. These results support a current field hypothesis that the neurophysiological effects of psychedelics underlying behavioral flexibility involve altering task-relevant activity in neural ensembles over subsequent days[79]. However, rather than simply accelerating or enhancing endogenous mechanisms of behavioral flexibility (*i.e.,* increasing activity in new ensembles), psilocy-

bin also engages an inhibitory mechanism of fear extinction. Indeed, the acute, response-predicting effects of psilocybin observed in this study are entirely comprised of inhibition of fear acquisition-associated neurons. Psilocybin's enhancement of extinction-like activity is not observed until the days following treatment and can be explained by prior suppression of fear memory-associated activity. Future research will explore how the neuroplastic effects of psilocybin on a cellular and circuit level evoke these distinct effects on neural dynamics and establish a causal relationship between the ensemble-specific changes in activity observed here with behavior.

Methods.

Experimental Methods.

Animals: Animals used in all studies were C57BL/6J mice *Animals:* Animals used in all studies were C57BL/6J mice from Jackson Laboratories (RRID: IMSR_JAX:000664). Mice were kept on a reverse 12-hour light/dark cycle. Behavior was performed at least 1 hour and no more than 4 hours following lights-off. Group-housed males (n=34) and females (n=16) between 8-12 weeks of age were used in the behavioral pharmacology experiment in Fig. 1. For the Miniscope study, males of 8-10 weeks of age underwent viral injection surgeries, followed by implantation of 4.0 (length) x 1.0mm (diameter) GRIN lens at 10-12 weeks, and behavior at 12-16 weeks (minimum 2-week recovery time from last surgery). Mice were singly housed following implant surgery.

TFC Conditioning and Extinction: One week prior to behavioral testing, Miniscope mice were habituated to the Miniscope for 2 days in 10 min sessions in the home cage. All mice underwent behavioral training and testing in Med Associates fear conditioning boxes for five days. In Context A, Med Associates chambers were equipped with smooth white floor inserts and cleaned with ethanol to provide a unique olfactory, tactile, and visual context. In Context B, the shock grid floor was exposed, mouse bedding was placed in a tray under the floor, and chambers were cleaned with Clidox. The five days of behavioral testing consisted of *Habituation* (Hab), *Acquisition* (Acq), and *Extinction 1-3* (Ext1-3). Hab and Ext1-3 took place in Context A, and *Acquisition* took place in Context B. The CS consisted of a 4kHz, 75dB tone delivered in 25, 200ms pips at 1Hz. During *Acquisition*, the CS was followed by a 20sec trace period preceding a 1mA, 2sec shock. On all other days, the shock was omitted. *Habituation* and *Acquisition* consisted of 8 trials, with jittered ITIs of 60±10sec. During *Extinction 1-3,* there were 6 trials per session. 30 minutes prior to *Extinction 1*, mice were injected with 1mg/kg psilocybin, contributed by the Elizabeth Heller Laboratory at the University of Pennsylvania, or saline. Mice were excluded from the study if they froze ≤20% of the time during *Acquisition* or ≤10% of the time during the first half of Extinction 1 (n=23 mice, Supplementary Fig. 1D). Two mice were excluded due to excessive barbering in the home-cage during the days of the experiment.

For Miniscope studies, a 2"-diameter hole was drilled in the top of a Med Associates box to feed the cables through. During the sessions, recordings were remotely controlled and streamed to a laptop for live monitoring. Recordings were made at LED power (0.7-1.5mW), gain (1.0-3.0), and focus (0-300μm) settings deemed appropriate for each mouse and kept as consistent between recording days as possible.

For the non-shock control condition, Miniscope-implanted mice underwent an identical protocol, except for the total omission of the shock.

Surgery: For Miniscope studies, all mice were unilaterally injected with 800nL of AAV9-syn-GCaMP8m-WPRE at a titer of 1.2e12 (Addgene virus #162375) in the RSC. RSC coordinates were chosen from past studies: -2.25 AP, +0.3ML,-0.8 DV. Mice were anesthetized with isoflurane. Hair was removed with Nair, and the skin sterilized with Betadine and ethanol. An incision was made with scissors along the scalp. Tissue was cleared from the skull surface using an air blast. The skull was leveled such that the Bregma-Lambda and ML DV difference was within ±0.1mm. A craniotomy was made at the chosen coordinates with a dental drill. A needle was lowered to the target coordinates through the craniotomy and virus infused at 100nL/min. The needle was left in the brain 10mins after infusion before being slowly withdrawn. The incision was sutured, and the animal was administered Meloxicam before being placed under a heat lamp for recovery.

Miniscope implantation surgeries subsequently followed the same protocol until the craniotomy step. A 1mm craniotomy was made by slowly widening the craniotomy with the dental drill. Dura was peeled back using microscissors, sharp forceps, and curved forceps. The craniotomy was regularly flushed with saline, and gel foam was applied to absorb blood. An Inscopix Pro-View Integrated GRIN lens and baseplate system was attached to the Miniscope and a stereotax. Using the Inscopix stereotax attachment, the lens was slowly lowered into a position over the injection site. The final DV coordinate was determined by assessing the view through the Miniscope stream. If tissue architecture could be observed in full focus with light fluctuations associated with RSC slow oscillatory activity under anesthesia, the lens was implanted at that coordinate (-0.6 to -0.3DV). The GRIN lens + baseplate system was secured to the skull with Metabond and then dental cement. After surgery, mice were singly housed and injected with Meloxicam for three consecutive days during recovery.

Miniscope validation: Before admission to the experiment, the miniscope was magnetically attached to each animal's implant for habituation and streamed using the Inscopix Data Acquisition Software. If many cells could be observed during spontaneous behavior in the home cage, the mouse was admitted. If only a few cells were visible, the session was recorded and analyzed in the Inscopix Data Processing Software (IDPS) to determine the number of observable cells. If an animal had >20 identifiable cells, they were admitted into the study. Others were euthanized.

Histology: Animals were perfused with 10% formalin and brains dissected. Brains were stored in formalin solution for 24 hours before being transferred to 30% sucrose. Brains were sectioned at 50μm on a cryostat and stored in PBS. RSC sections were stained with DAPI and sections from -2.18AP to -2.88AP were mounted on slides. The section with the deepest and widest GRIN lens track was designated as the coordinate of implant.

Analysis Methods.

Behavioral: Behavior was recorded by Basler cameras into Pylon Viewer at 15Hz. Videos were then processed in the open source ezTrack Jupyter Notebook. The algorithm was calibrated to the standard light fluctuations in the empty chambers and the empty chambers with the Miniscope wire dangling in them for each respective study. A freezing threshold was determined in terms of number of pixels changed/frame by visually validating portions of videos classified as "Freezing" or "Moving" by the algorithm. In

general, a freezing threshold of 50-200pixels/frame was used in non-Miniscope studies, whereas a threshold of 300pixels/frame was used in all Miniscope animals, necessitated by movements of the Miniscope wire. An animal was only classified as "Freezing" if the pixels/frame remained below threshold for at least 1sec, or 15 frames. Freezing status per frame was exported in a CSV file and post-processed in Matlab to calculate % freezing windows of time. Freezing plotted here is % freezing during the trace period, as this is the interval of time invoking the RSC for fear and extinction encoding and retrieval. Freezing videos were aligned to trial times by beginning analysis at the first frame of the red light in the Med Associates boxes switching on, indicating session start. Although tone delivery times were pseudo-random with respect to the animals, they were hard-coded by the experimenter, so analysis alignment to session start was sufficient to align video to tone.

Calcium imaging pre-processing: Videos were downloaded from the Inscopix Data Acquisition Box and uploaded to the Inscopix Data Processing Software (IDPS). Videos were spatially downsampled by a factor of 4 and spatial bandpass filtered between 0.005 and 0.500. Videos were then motion corrected with respect to their mean frame. Cells were identified and extracted using CNFM-E (default parameters in the Inscopix implementation of CNMF-E, except the minimum in-line pixel correlation = 0.7 and minimum signal to noise ratio = 7.0) and second-order deconvolved using SCS. Videos across 5 days of behavioral training were longitudinally registered in IDPS (minimum normalized cross-correlation = 0.1). Only cells registered on all 5 days were considered for further analysis.

Calcium imaging post-processing: Most subsequent analysis was performed in custom Matlab scripts, available in the associated GitHub. Deconvolved calcium traces of cells from each session were aligned according to their global cell index determined in longitudinal registration. As the window considered for each trial included a 10sec baseline period, a 25sec stim period, a 20 sec trace period, a 2 sec shock/omission period, and 3 sec after, each trial was 60sec. Neural activity was therefore summed within 1 sec time windows. Miniscope recordings were started exactly 30.00sec before behavioral session start, and this information was used to align data to behavior and neural data. To determine whether a cell was stimuli-, trace-, and/or shock-responsive, their baseline period activity was compared to their activity during the period of interest by permutation test in 1000 iterations. The proportion of stim/trace/shock-responsive cells compared to all longitudinally registered cells recorded within an animal was calculated for each session and compared between groups and over time with a Two-Way RM ANOVA. When all recorded cells were considered, proportions of these cells compared to the total population were compared within session across groups with a Two-Way ANOVA. A cell was considered stable if it was responsive in both the first and last two trials of a given session; recruited if it was not responsive in the first two but responsive in the last two; and suppressed if the opposite was true. Pearson's rho was used to calculate the correlations between the proportion of these cells and total % freezing in a session. To calculate the change of activity in groups of neurons between sessions, activity was z-scored to traces recorded in *Acquisition* and compared between groups and over time with a Two-Way RM ANOVA. To calculate overlaps between ensembles of neurons, ensembles were identified by TCA (described below) in each animal. Whether these overlaps were small or large was determined by a Wilcoxon rank-sum test comparing the median of each overlap in each group with a 50% threshold. If an ensemble shared significantly <50% of

neurons with another, this was considered a small overlap. All statistics were calculated in Prism.

Freezing encoding: To calculate freezing encoding in single longitudinally registered neurons, neural traces were downsampled from 20 to 15Hz and aligned to a 15Hz binary freezing trace. A binomial GLM was trained on half of the data from each session and evaluated on the other half to generate auROCs. The mean auROC of all neurons in a mouse in each session was reported in the main text. To determine the population encoding of freezing in the RSC, 15Hz activity of each recorded cell was normalized to its maximum. 15Hz PSTHs from 2 seconds before to 2 seconds freezing onset or freezing offset of all cells from each day were averaged over trials and projected into the same principal component space, unique to each animal. The Euclidean distance was calculated between these trajectories at each timepoint and averaged across groups for Fig. 3D and then averaged over time for Fig. 3E. To determine whether changes in freezing encoding in PC space were observable at the single cell level, d-prime was calculated for each neuron over the same motion and freezing time windows used to produce the trajectories. Where a = activity:

$$ d' = \frac{\overline{a_{freezing}} - \overline{a_{motion}}}{\overline{a_{freezing}} + \overline{a_{motion}}} $$

Single cell freezing discrimination for each animal was reported as the median of the absolute values of d-prime. These outcomes were compared within sessions between treatment and extinction rate groups with a Two-Way ANOVA.

TCA: To perform TCA, post-processed calcium imaging data was arranged into tensors t_{sec} x c_{cells} x T_{trials} in size for each animal, exported as a Matlab structure, and imported into Spyder where we employed the TensorTools package developed by Williams et al., 2018. To determine the appropriate model rank empirically, TCA was first run on the pooled and aligned tensors from all mice in each treatment group, and model reconstruction error and similarity were plotted as a function of increasing model rank. The elbow method revealed that models of rank 5 were most appropriate for subsequent analysis (Reconstruction error = 0.615; Model similarity between four iterations = 1). Models of rank 5 were then generated for each animal.

To measure the dominance of each of the 5 components during a given trial, the relative strength of a given component was measured as the fraction of the total trial weights at that time assigned to that given component. This measure functions to assess how dominant this component is over others at a certain time. Linear regression was used to determine the relationship between component-dominance and behavior over time.

To determine total extent of session discriminability of TCA-identified components, pooled TCA models were generated 100 times for each group and compared to models generated on 100 shuffled datasets from the same groups using unpaired t-tests. Neurons were randomly shuffled at each timepoint to preserve the within- and across-trial temporal structure of the data, controlling for changes in recording quality across days. To compare across groups, neurons were randomly subsampled in each iteration of TCA to control for effects of the number of cells on session discriminability.

As TCA also assigns weights to each neuron in each component, we found we could use this information to identify ensembles of neurons driving each component.

Identifying neural ensembles: TCA returns neuron factor loadings signifying the relative weight of each neuron in each component.

However, the absolute values of these weights are influenced by the size of the data tensor across all three dimensions. To determine the neuron factor loading or weight above which a neuron would be contributing to a component greater than by chance, simulated data tensors were generated for each animal populated with identically behaving neurons. For animal a with c longitudinally recorded neurons, given a constant experimental structure of T = 34 total trials with t = 60 sec per trial, a tensor of 60 sec x c_a x 34 trials was generated and TCA iterated 100x. We chose a threshold of w=1.0 as the median and mean of the null distribution of the factor loading threshold were greater than 1.0 and less than 1.1. Primary outcomes (See **Fig. 5B-D, Supplementary Fig. 6**) were re-calculated using various factor thresholds to verify that results with a threshold w=1.0 are robust to threshold choice. Thus, *Acq*-dominant ensemble, for instance, was therefore comprised of neurons with w>1 in the *Acq*-dominant component determined by the strength metric described above.

Multiple regression: To determine the predictive power of the observed changes in neural ensemble activity over freezing in late Extinction 3, mean % trace period freezing, mean change in activity from Acquisition of the *Acq*-dominant ensemble during Extinction 1 and of the *Ext3*-dominant ensemble during Extinction 3 were all respectively z-scored within treatment condition to normalize the distributions and regressed. Adjusted R^2, p values, coefficients, and their 95% confidence intervals are reported.

Fisher linear discriminant analysis: A Fisher decoder was trained in Matlab on one of seven predictors: the mean activity of the *Acq-Only, Ext1-Only, Ext3-Only, Acq/Ext1, Acq/Ext3, Ext1/Ext3*, or *Acq/Ext1/Ext3* ensembles over all timepoints in each session. Class labels were "Responders," "Non-responders," or "Rapid" mice. Fisher decoders were trained to distinguish between data from two of the class labels to determine how similar or different the ensembles between pairs of groups behaved. Fisher decoders were trained on a randomly selected 50% of the data and evaluated on the other 50% over 100 iterations. As a control, class labels were randomly shuffled, and model performance was evaluated on the shuffled data. If the accuracies of the decoders generated by a given ensemble's activity overlapped with the distribution of accuracies when evaluated on shuffled data, it was classified as failing to predict responder status or treatment. If not, then this ensemble was classified as predictive with respect to the given distinction. To validate the ability to distinguish all three classes based on these ensembles was verified with three-way Fisher decoders in Supplementary Fig. 4.

Computational model: A linear non-linear firing rate model was composed of a hypothesized RSC microcircuit comprised of *Acq*- and *Ext3*-dominant neurons obeying the following system of equations based on the cortical circuit model proposed by Park and Geffen, 2022[80]. To evaluate the activity at time t in neuron I, take the following quantities as time t-1:

$$\frac{dI}{dt} = (w_{i,j} \cdot A_j - w_{i,o} \cdot A_o + w_{i,s} \cdot S - I) * tau$$

$$F_i(dI) \begin{cases} 0 & if \quad dI < 0 \\ r * dI & if \quad 0 < dI < 1 \\ 1 & if \quad dI > 1/r \end{cases}$$

$$\frac{dA}{dt} = (F_i - A_i) * tau$$

Where I is the synaptic input to neuron i, w_{ij} is the weight of input from neuron j in the same ensemble, $w_{i,o}$ is the weight of input from neuron o in the opposing ensemble, A is the presynaptic neuron's

activity, $w_{i,s}$ is the neuron's selectivity matrix for the stimulus, S is the stimulus matrix for tone, trace, and shock/omission inputs, and tau is the time constant (1ms where dt is 1s). F is the function describing the nonlinear part of neural activation, such that subthreshold inputs are scaled by a factor r = 3. The transformed synaptic input F is then added to the neuron's activity A.

Each ensemble was modeled with 10 recurrently connected units with either selective or mixed-selective response properties mimicking the real data that mutually inhibit neurons of the opposite ensemble. (*Acq*-dominant ensemble: 80% shock-responsive, 20% tone responsive, 20% trace responsive; *Ext3*-dominant ensemble: 50% shock-responsive, 30% tone responsive, 40% trace responsive). Intra-ensemble weights underwent excitatory plasticity according to a Hebbian learning rule of where the learning rate alpha = 0.1. Psilocybin was simulated only as 100 increasing amounts of direct synaptic inhibition ranging between 0 and 1.

The model was trained on an identical TFC acquisition and extinction task as the mice, with tone and trace delivery simulated as of 0.1 to their responsive units. Shock or shock omission were modeled as inputs to shock or omission responsive neurons as an input of 1 or -1 respectively, and omission-responsive Ext3-dominant neurons weighted this input with w=-1 to flip the sign. The difference in magnitude between shock and tone or trace inputs is intended to reflect their differing salience. The magnitude of the shock-omission input decreased linearly with each trial after Extinction 1, intended to represent reduced salience of the absence of shock over time.

To test the model, its structure was systematically varied to challenge the following underlying assumptions: 1) to test whether the neural populations are excitatory, the weight matrices between neurons of the same ensemble were set to zero, one by one and then together; 2) to test whether the neural populations were mutually inhibitory, the input weights from one ensemble to the other were set to zero, one by one and then together; 3) to test whether shock-omission sensitivity was required, the weight of shock omission inputs to the *Ext3*-dominant ensemble was set to zero.

To test whether inhibition of the *Acq*-dominant ensemble was sufficient to explain our empirical results, psilocybin was simulated as P = 101 evenly incremented values of 0 to 100 and subtracted directly from the synaptic input dI as $P*tau$ for the whole Extinction 1 epoch of training.

To determine the fit between the output activities of the model and the real data, the slopes of their linear parts were calculated using the line equation:

$$\frac{dx}{dy} = m$$

MSE between the real data and each slope was then calculated. To calculate simulated freezing in the model, activities were plugged into the equation yielded from the multiple regression of z-score % freezing on z-score activity of *Acq*-dominant neurons during Extinction 1 and *Ext3*-dominant neurons during Extinction 3:

$$Normalized \% \, Trace \, Period \, Freezing = 0.4977 * A_{Acq,Ext1} - 0.6111 * A_{Ext3,Ext3}$$

References.

1. Hoppen, Thole H, Stefan Priebe, Inja Vetter, and Nexhmedin Morina. "Global Burden of Post-Traumatic Stress Disorder and Major Depression in Countries Affected by War between 1989 and 2019: A Systematic Review and Meta-Analysis." *BMJ Global Health* 6, no. 7 (July 2021): e006303. https://doi.org/10.1136/bmjgh-2021-006303.

2. Nutt, David, and Robin Carhart-Harris. "The Current Status of Psychedelics in Psychiatry." *JAMA Psychiatry* 78, no. 2 (February 1, 2021): 121–22. https://doi.org/10.1001/jamapsychiatry.2020.2171.

3. Griffiths, R. R., M.W. Johnson, W. A. Richards, B.D. Richards, U. McCann, and R. Jesse. "Psilocybin Occasioned Mystical-Type Experiences: Immediate and Persisting Dose-Related Effects." *Psychopharmacology* 218, no. 4 (December 2011): 649–65. https://doi.org/10.1007/s00213-011-2358-5.

4. Agin-Liebes, Gabrielle I, Tara Malone, Matthew M Yalch, Sarah E Mennenga, K Linnae Ponté, Jeffrey Guss, Anthony P Bossis, Jim Grigsby, Stacy Fischer, and Stephen Ross. "Long-Term Follow-up of Psilocybin-Assisted Psychotherapy for Psychiatric and Existential Distress in Patients with Life-Threatening Cancer." *Journal of Psychopharmacology* 34, no. 2 (February 1, 2020): 155–66. https://doi.org/10.1177/0269881119897615.

5. Aday, Jacob S., Cayla M. Mitzkovitz, Emily K. Bloesch, Christopher C. Davoli, and Alan K. Davis. "Long-Term Effects of Psychedelic Drugs: A Systematic Review." *Neuroscience & Biobehavioral Reviews* 113 (June 1, 2020): 179–89. https://doi.org/10.1016/j.neubiorev.2020.03.017.

6. Gukasyan, Natalie, Alan K Davis, Frederick S Barrett, Mary P Cosimano, Nathan D Sepeda, Matthew W Johnson, and Roland R Griffiths. "Efficacy and Safety of Psilocybin-Assisted Treatment for Major Depressive Disorder: Prospective 12-Month Follow-Up." *Journal of Psychopharmacology* 36, no. 2 (February 1, 2022): 151–58. https://doi.org/10.1177/02698811211073759.

7. Hesselgrave, Natalie, Timothy A. Troppoli, Andreas B. Wulff, Anthony B. Cole, and Scott M. Thompson. "Harnessing Psilocybin: Antidepressant-like Behavioral and Synaptic Actions of Psilocybin Are Independent of 5-HT2R Activation in Mice." *Proceedings of the National Academy of Sciences of the United States of America* 118, no. 17 (April 27, 2021): e2022489118. https://doi.org/10.1073/pnas.2022489118.

8. Cameron, Lindsay P., Seona D. Patel, Maxemiliano V. Vargas, Eden V. Barragan, Hannah N. Saeger, Hunter T. Warren, Winston L. Chow, John A. Gray, and David E. Olson. "5-HT2ARs Mediate Therapeutic Behavioral Effects of Psychedelic Tryptamines." *ACS Chemical Neuroscience* 14, no. 3 (February 1, 2023): 351–58. https://doi.org/10.1021/acschemneuro.2c00718.

9. Hibicke, Meghan, Hannah M. Kramer, and Charles D. Nichols. "A Single Administration of Psilocybin Persistently Rescues Cognitive Deficits Caused by Adolescent Chronic Restraint Stress Without Long-Term Changes in Synaptic Protein Gene Expression in a Rat Experimental System with Translational Relevance to Depression." *Psychedelic Medicine*, March 3, 2023. https://doi.org/10.1089/psymed.2022.0012.

10. Hernandez-Leon, Alberto, Raúl Iván Escamilla-Orozco, Aylín R. Tabal-Robles, David Martínez-Vargas, Leticia Romero-Bautista, Gerson Escamilla-Soto, Osiris S. González-Romero, Martín Torres-Valencia, and María Eva González-Trujano. "Antidepressant- and Anxiolytic-like Activities and Acute Toxicity Evaluation of the Psilocybe Cubensis Mushroom in Experimental Models in Mice." *Journal of Ethnopharmacology* 320 (February 10, 2024): 117415. https://doi.org/10.1016/j.jep.2023.117415.

11. Jones, Nathan T, Zarmeen Zahid, Sean M Grady, Ziyad W Sultan, Zhen Zheng, Matthew I Banks, and Cody J Wenthur. "Delayed Anxiolytic-Like Effects of Psilocybin in Male Mice Are Supported by Acute Glucocorticoid Release." Preprint. Animal Behavior and Cognition, August 14, 2020. https://doi.org/10.1101/2020.08.12.248229.

12. Jones, Nathan T., Zarmeen Zahid, Sean M. Grady, Ziyad W. Sultan, Zhen Zheng, John Razidlo, Matthew I. Banks, and Cody J. Wenthur. "Transient Elevation of Plasma Glucocorticoids Supports Psilocybin-Induced Anxiolysis in Mice." *ACS Pharmacology & Translational Science* 6, no. 8 (August 11, 2023): 1221–31. https://doi.org/10.1021/acsptsci.3c00123.

13. Takaba, Rika, Daisuke Ibi, Keisuke Yoshida, Eri Hosomi, Ririna Kawase, Hiroko Kitagawa, Hirotaka Goto, et al. "Ethopharmacological Evaluation of Antidepressant-like Effect of Serotonergic Psychedelics in C57BL/6J Male Mice." *Naunyn-Schmiedeberg's Archives of Pharmacology*, October 24, 2023. https://doi.org/10.1007/s00210-023-02778-x.

14. Odland, Anna U., Jesper L. Kristensen, and Jesper T. Andreasen. "Investigating the Role of 5-HT2A and 5-HT2C Receptor Activation in the Effects of Psilocybin, DOI, and Citalopram on Marble Burying in Mice." *Behavioural Brain Research* 401 (March 5, 2021): 113093. https://doi.org/10.1016/j.bbr.2020.113093.

15. Wulff, Andreas B., Charles D. Nichols, and Scott M. Thompson. "Preclinical Perspectives on the Mechanisms Underlying the Therapeutic Actions of Psilocybin in Psychiatric Disorders." *Neuropharmacology* 231 (June 15, 2023): 109504. https://doi.org/10.1016/j.neuropharm.2023.109504.

16. Passie, Torsten, Juergen Seifert, Udo Schneider, and Hinderk M. Emrich. "The Pharmacology of Psilocybin." *Addiction Biology* 7, no. 4 (2002): 357–64. https://doi.org/10.1080/1355621021000005937.

17. Lowe, Henry, Ngeh Toyang, Blair Steele, Henkel Valentine, Justin Grant, Amza Ali, Wilfred Ngwa, and Lorenzo Gordon. "The Therapeutic Potential of Psilocybin." *Molecules (Basel, Switzerland)* 26, no. 10 (May 15, 2021): 2948. https://doi.org/10.3390/molecules26102948.

18. Garcia-Romeu, Albert, Roland R. Griffiths, and Matthew W. Johnson. "Psilocybin-Occasioned Mystical Experiences in the Treatment of Tobacco Addiction." *Current Drug Abuse Reviews* 7, no. 3 (2015): 157–64.

19. Bremler, Rebecka, Nancy Katati, Parvinder Shergill, David Erritzoe, and Robin L. Carhart-Harris. "Case Analysis of Long-Term Negative Psychological Responses to Psychedelics." *Scientific Reports* 13 (September 25, 2023): 15998. https://doi.org/10.1038/s41598-023-41145-x.

20. Simonsson, Otto, Per Carlbring, Robin Carhart-Harris, Alan K. Davis, David J. Nutt, Roland R. Griffiths, David Erritzoe, and Simon B. Goldberg. "Assessing the Risk of Symptom Worsening in

Psilocybin-Assisted Therapy for Depression: A Systematic Review and Individual Participant Data Meta-Analysis." *Psychiatry Research* 327 (September 1, 2023): 115349. https://doi.org/10.1016/j.psychres.2023.115349.

21. Simonsson, Otto, Peter S. Hendricks, Richard Chambers, Walter Osika, and Simon B. Goldberg. "Prevalence and Associations of Challenging, Difficult or Distressing Experiences Using Classic Psychedelics." *Journal of Affective Disorders* 326 (April 1, 2023): 105–10. https://doi.org/10.1016/j.jad.2023.01.073.

22. Breeksema, Joost J, Bouwe W Kuin, Jeanine Kamphuis, Wim van den Brink, Eric Vermetten, and Robert A Schoevers. "Adverse Events in Clinical Treatments with Serotonergic Psychedelics and MDMA: A Mixed-Methods Systematic Review." *Journal of Psychopharmacology (Oxford, England)* 36, no. 10 (October 2022): 1100–1117. https://doi.org/10.1177/02698811221116926.

23. Lewis, Candace R., Katrin H. Preller, B. Blair Braden, Cory Riecken, and Franz X. Vollenweider. "Rostral Anterior Cingulate Thickness Predicts the Emotional Psilocybin Experience." *Biomedicines* 8, no. 2 (February 18, 2020):

24. Halim, Haniya J., Bradley G. Burk, Rachel E. Fargason, and Badari Birur. "Manic Episode Following Psilocybin Use in a Man with Bipolar II Disorder: A Case Report." *Frontiers in Psychiatry* 14 (2023): 1221131. https://doi.org/10.3389/fpsyt.2023.1221131.

25. Davis, Alan K., Frederick S. Barrett, and Roland R. Griffiths. "Psychological Flexibility Mediates the Relations between Acute Psychedelic Effects and Subjective Decreases in Depression and Anxiety." *Journal of Contextual Behavioral Science* 15 (January 2020): 39–45. https://doi.org/10.1016/j.jcbs.2019.11.004.

26. Doss, Manoj K., Michal Považan, Monica D. Rosenberg, Nathan D. Sepeda, Alan K. Davis, Patrick H. Finan, Gwenn S. Smith, et al. "Psilocybin Therapy Increases Cognitive and Neural Flexibility in Patients with Major Depressive Disorder." *Translational Psychiatry* 11, no. 1 (November 8, 2021): 574. https://doi.org/10.1038/s41398-021-01706-y.

27. Pacheco, Alejandro Torrado, Randall J. Olson, Gabriela Garza, and Bita Moghaddam. "Acute Psilocybin Enhances Cognitive Flexibility in Rats." bioRxiv, January 9, 2023. https://doi.org/10.1101/2023.01.09.523291.

28. Conn, K., L. K. Milton, K. Huang, H. Munguba, J. Ruuska, M. B. Lemus, E. Greaves, J. Homman-Ludiye, B. J. Oldfield, and C. J. Foldi. "Psilocybin Prevents Activity-Based Anorexia in Female Rats by Enhancing Cognitive Flexibility: Contributions from 5-HT1A and 5-HT2A Receptor Mechanisms." bioRxiv, December 13, 2023. https://doi.org/10.1101/2023.12.12.571374.

29. Price, Rebecca B., and Ronald Duman. "Neuroplasticity in Cognitive and Psychological Mechanisms of Depression: An Integrative Model." *Molecular Psychiatry* 25, no. 3 (March 2020): 530–43. https://doi.org/10.1038/s41380-019-0615-x.

30. Zhukovsky, Peter, Johan Alsiö, Bianca Jupp, Jing Xia, Chiara Guiliano, Lucy Jenner, Jessica Griffiths, et al. "Perseveration in a Spatial-Discrimination Serial Reversal Learning Task Is Differentially Affected by MAO-A and MAO-B Inhibition and Associated with Reduced Anxiety and Peripheral Serotonin Levels." *Psychopharmacology* 234, no. 9 (2017): 1557–71. https://doi.org/10.1007/s00213-017-4569-x.

31. Vargas, Maximiliano V., Lee E. Dunlap, Chunyang Dong, Samuel J. Carter, Robert J. Tombari, Shekib A. Jami, Lindsay P. Cameron, et al. "Psychedelics Promote Neuroplasticity through the Activation of Intracellular 5-HT2A Receptors." *Science* 379, no. 6633 (February 17, 2023): 700–706. https://doi.org/10.1126/science.adf0435.

32. Carhart-Harris, R. L., and K. J. Friston. "REBUS and the Anarchic Brain: Toward a Unified Model of the Brain Action of Psychedelics." Edited by Eric L. Barker. *Pharmacological Reviews* 71, no. 3 (July 2019): 316–44. https://doi.org/10.1124/pr.118.017160.

33. Alonso, Joan Francesc, Sergio Romero, Miquel Àngel Mañanas, and Jordi Riba. "Serotonergic Psychedelics Temporarily Modify Information Transfer in Humans." *International Journal of Neuropsychopharmacology* 18, no. 8 (June 2015). https://doi.org/10.1093/ijnp/pyv039.

34. Ly, Calvin, Alexandra C. Greb, Lindsay P. Cameron, Jonathan M. Wong, Eden V. Barragan, Paige C. Wilson, Kyle F. Burbach, et al. "Psychedelics Promote Structural and Functional Neural Plasticity." *Cell Reports* 23, no. 11 (June 12, 2018): 3170–82. https://doi.org/10.1016/j.celrep.2018.05.022.

35. Olson, David E. "Psychoplastogens: A Promising Class of Plasticity-Promoting Neurotherapeutics." *Journal of Experimental Neuroscience* 12 (January 1, 2018): 1179069518800508. https://doi.org/10.1177/1179069518800508.

36. Shao, Ling-Xiao, Clara Liao, Ian Gregg, Pasha A. Davoudian, Neil K. Savalia, Kristina Delagarza, and Alex C. Kwan. "Psilocybin Induces Rapid and Persistent Growth of Dendritic Spines in Frontal Cortex in Vivo." *Neuron* 109, no. 16 (August 18, 2021): 2535-2544.e4. https://doi.org/10.1016/j.neuron.2021.06.008.

37. Ly, Calvin, Alexandra C. Greb, Maximiliano V. Vargas, Whitney C. Duim, Ana Cristina G. Grodzki, Pamela J. Lein, and David E. Olson. "Transient Stimulation with Psychoplastogens Is Sufficient to Initiate Neuronal Growth." *ACS Pharmacology & Translational Science* 4, no. 2 (April 9, 2021): 452–60. https://doi.org/10.1021/acsptsci.0c00065.

38. Du, Yingjie, Yunfeng Li, Xiangting Zhao, Yishan Yao, Bin Wang, Liming Zhang, and Guyan Wang. "Psilocybin Facilitates Fear Extinction in Mice by Promoting Hippocampal Neuroplasticity." *Chinese Medical Journal*, March 30, 2023. https://doi.org/10.1097/CM9.0000000000002647.

39. Moliner, Rafael, Mykhailo Girych, Cecilia A. Brunello, Vera Kovaleva, Caroline Biojone, Giray Enkavi, Lina Antenucci, et al. "Psychedelics Promote Plasticity by Directly Binding to BDNF Receptor TrkB." *Nature Neuroscience* 26, no. 6 (June 2023): 1032–41. https://doi.org/10.1038/s41593-023-01316-5.

40. Schmitz, Gavin P., Yi-Ting Chiu, Gabriele M. König, Evi Kostenis, Bryan L. Roth, and Melissa A. Herman. "Psychedelic Compounds Directly Excite 5-HT2A Layer 5 Pyramidal Neurons in the Prefrontal Cortex through a 5-HT2A Gq -Mediated Activation Mechanism." bioRxiv, November 15, 2022. https://doi.org/10.1101/2022.11.15.516655.

41. Vann, Seralynne D., John P. Aggleton, and Eleanor A. Maguire. "What Does the Retrosplenial Cortex Do?" *Nature Reviews Neuroscience* 10, no. 11 (November 2009): 792–802. https://doi.org/10.1038/nrn2733.

42. Summerfield, Jennifer J., Demis Hassabis, and Eleanor A. Maguire. "Cortical Midline Involvement in Autobiographical Memory." *Neuroimage* 44, no. 3 (February 1, 2009): 1188–1200. https://doi.org/10.1016/j.neuroimage.2008.09.033.

43. Maguire, E A. "Neuroimaging Studies of Autobiographical Event Memory." *Philosophical Transactions of the Royal Society of London. Series B* 356, no. 1413 (September 29, 2001): 1441–51. https://doi.org/10.1098/rstb.2001.0944.

44. Todd, Travis P., Nicole E. DeAngeli, Matthew Y. Jiang, and David J. Bucci. "Retrograde Amnesia of Contextual Fear Conditioning: Evidence for Retrosplenial Cortex Involvement in Configural Processing." *Behavioral Neuroscience* 135 (2021): 453–61. https://doi.org/10.1037/bne0000432.

45. Todd, Travis P., and David J. Bucci. "Retrosplenial Cortex and Long-Term Memory: Molecules to Behavior." *Neural Plasticity* 2015 (2015): 414173. https://doi.org/10.1155/2015/414173.

46. Miller, Adam M P, Anna C Serrichio, and David M Smith. "Dual-Factor Representation of the Environmental Context in the Retrosplenial Cortex." *Cerebral Cortex* 31, no. 5 (May 1, 2021): 2720–28. https://doi.org/10.1093/cercor/bhaa386.

47. Hattori, Ryoma, and Takaki Komiyama. "Context-Dependent Persistency as a Coding Mechanism for Robust and Widely Distributed Value Coding." *Neuron* 110, no. 3 (February 2022): 502-515.e11. https://doi.org/10.1016/j.neuron.2021.11.001.

48. Sun, Weilun, Ilseob Choi, Stoyan Stoyanov, Oleg Senkov, Evgeni Ponimaskin, York Winter, Janelle M. P. Pakan, and Alexander Dityatev. "Context Value Updating and Multidimensional Neuronal Encoding in the Retrosplenial Cortex." *Nature Communications* 12, no. 1 (October 18, 2021): 6045. https://doi.org/10.1038/s41467-021-26301-z.

49. Trask, Sydney, Nicole C. Ferrara, Aaron M. Jasnow, and Janine L. Kwapis. "Contributions of the Rodent Cingulate-Retrosplenial Cortical Axis to Associative Learning and Memory: A Proposed

Circuit for Persistent Memory Maintenance." *Neuroscience & Biobehavioral Reviews* 130 (November 2021): 178–84. https://doi.org/10.1016/j.neubiorev.2021.08.023.

50. Trask, Sydney, and Fred J Helmstetter. "Unique Roles for the Anterior and Posterior Retrosplenial Cortices in Encoding and Retrieval of Memory for Context." *Cerebral Cortex* 32, no. 17 (August 22, 2022): 3602–10. https://doi.org/10.1093/cercor/bhab436.

51. Sousa, André F. de, Kiriana K. Cowansage, Ipshita Zutshi, Leonardo M. Cardozo, Eun J. Yoo, Stefan Leutgeb, and Mark Mayford. "Optogenetic Reactivation of Memory Ensembles in the Retrosplenial Cortex Induces Systems Consolidation." *Proceedings of the National Academy of Sciences* 116, no. 17 (April 23, 2019): 8576–81. https://doi.org/10.1073/pnas.1818432116.

52. Mitchell, Anna S., Rafal Czajkowski, Ningyu Zhang, Kate Jeffery, and Andrew J. D. Nelson. "Retrosplenial Cortex and Its Role in Spatial Cognition." *Brain and Neuroscience Advances* 2 (2018): 2398212818757098.
https://doi.org/10.1177/2398212818757098.

53. Brennan, Ellen KW, Izabela Jedrasiak-Cape, Sameer Kailasa, Sharena P Rice, Shyam Kumar Sudhakar, and Omar J Ahmed. "Thalamus and Claustrum Control Parallel Layer 1 Circuits in Retrosplenial Cortex." *eLife* 10 (June 25, 2021): e62207. https://doi.org/10.7554/eLife.62207.

54. Cheng, Ning, Qiqi Dong, Zhen Zhang, Li Wang, Xiaojing Chen, and Cheng Wang. "Egocentric Processing of Items in Spines, Dendrites, and Somas in the Retrosplenial Cortex." *Neuron* 0, no. 0 (December 14, 2023). https://doi.org/10.1016/j.neuron.2023.11.018.

55. Carhart-Harris, Robin L., Suresh Muthukumaraswamy, Leor Roseman, Mendel Kaelen, Wouter Droog, Kevin Murphy, Enzo Tagliazucchi, et al. "Neural Correlates of the LSD Experience Revealed by Multimodal Neuroimaging." *Proceedings of the National Academy of Sciences* 113, no. 17 (April 26, 2016): 4853–58. https://doi.org/10.1073/pnas.1518377113.

56. Wang, Guangyu, Hong Xie, Lun Wang, Wenhan Luo, Yixiang Wang, Jun Jiang, Chun Xiao, Feng Xing, and Ji-Song Guan. "Switching From Fear to No Fear by Different Neural Ensembles in Mouse Retrosplenial Cortex." *Cerebral Cortex* 29, no. 12 (December 17, 2019): 5085–97. https://doi.org/10.1093/cercor/bhz050.

57. Zhang, Kai, Dan Shen, Shihao Huang, Javed Iqbal, Gengdi Huang, Jijian Si, Yanxue Xue, and Jian-Li Yang. "The Sexually Divergent cFos Activation Map of Fear Extinction." *Heliyon* 10, no. 1 (January 15, 2024): e23748. https://doi.org/10.1016/j.heliyon.2023.e23748.

58. Davoudian, Pasha A., Ling-Xiao Shao, and Alex C. Kwan. "Shared and Distinct Brain Regions Targeted for Immediate Early Gene Expression by Ketamine and Psilocybin." *ACS Chemical Neuroscience* 14, no. 3 (February 1, 2023): 468–80. https://doi.org/10.1021/acschemneuro.2c00637.

59. Kometer, Michael, André Schmidt, Lutz Jäncke, and Franz X. Vollenweider. "Activation of Serotonin 2A Receptors Underlies the Psilocybin-Induced Effects on α Oscillations, N170 Visual-Evoked Potentials, and Visual Hallucinations." *Journal of Neuroscience* 33, no. 25 (June 19, 2013): 10544–51. https://doi.org/10.1523/JNEUROSCI.3007-12.2013.

60. Liu, Shijing, Marcy J. Bubar, Maria Fe Lanfranco, Gilbert R. Hillman, and Kathryn A. Cunningham. "Serotonin2C Receptor (5-HT2CR) Localization in GABA Neurons of the Rat Medial Prefrontal Cortex: Implications for Understanding the Neurobiology of Addiction." *Neuroscience* 146, no. 4 (June 8, 2007): 1677–88. https://doi.org/10.1016/j.neuroscience.2007.02.064.

61. Pompeiano, M., J. M. Palacios, and G. Mengod. "Distribution of the Serotonin 5-HT2 Receptor Family mRNAs: Comparison between 5-HT2A and 5-HT2C Receptors." *Molecular Brain Research* 23, no. 1 (April 1, 1994): 163–78. https://doi.org/10.1016/0169-328X(94)90223-2.

62. Zhang, Yajuan, Chu-Chung Huang, Jiajia Zhao, Yuchen Liu, Mingrui Xia, Xiaoqin Wang, Dongtao Wei, et al. "Resting-State Functional Connectivity of the Raphe Nuclei in Major Depressive Disorder: A Multi-Site Study." *NeuroImage : Clinical* 37 (February 24, 2023): 103359. https://doi.org/10.1016/j.nicl.2023.103359.

63. Corcoran, Kevin A., Michael D. Donnan, Natalie C. Tronson, Yomayra F. Guzmán, Can Gao, Vladimir Jovasevic, Anita L. Guedea, and Jelena Radulovic. "NMDA Receptors in Retrosplenial Cortex Are Necessary for Retrieval of Recent and Remote Context Fear Memory." *The Journal of Neuroscience* 31, no. 32 (August 10, 2011): 11655–59. https://doi.org/10.1523/JNEUROSCI.2107-11.2011.

64. Corcoran, Kevin A., Brendan J. Frick, Jelena Radulovic, and Leslie M. Kay. "Analysis of Coherent Activity between Retrosplenial Cortex, Hippocampus, Thalamus, and Anterior Cingulate Cortex during Retrieval of Recent and Remote Context Fear Memory." *Neurobiology of Learning and Memory* 127 (January 2016): 93–101. https://doi.org/10.1016/j.nlm.2015.11.019.

65. Auguste, Anne, Nicolas Fourcaud-Trocmé, David Meunier, Alexandra Gros, Samuel Garcia, Belkacem Messaoudi, Marc Thevenet, Nadine Ravel, and Alexandra Veyrac. "Distinct Brain Networks for Remote Episodic Memory Depending on Content and Emotional Value." bioRxiv, September 19, 2022. https://doi.org/10.1101/2022.09.16.508241.

66. Todd, Travis P., Max L. Mehlman, Christopher S. Keene, Nicole E. DeAngeli, and David J. Bucci. "Retrosplenial Cortex Is Required for the Retrieval of Remote Memory for Auditory Cues." *Learning & Memory* 23, no. 6 (June 2016): 278–88. https://doi.org/10.1101/lm.041822.116.

67. Fournier, Danielle I., Han Yin Cheng, Armin Tavakkoli, Allan T. Gulledge, David J. Bucci, and Travis P. Todd. "Retrosplenial Cortex Inactivation during Retrieval, but Not Encoding, Impairs Remotely Acquired Auditory Fear Conditioning in Male Rats." *Neurobiology of Learning and Memory* 185 (November 2021): 107517. https://doi.org/10.1016/j.nlm.2021.107517.

68. Kwapis, Janine L., Timothy J. Jarome, Jonathan L. Lee, Marieke R. Gilmartin, and Fred J. Helmstetter. "Extinguishing Trace Fear Engages the Retrosplenial Cortex Rather than the Amygdala." *Neurobiology of Learning and Memory* 113 (September 2014): 41–54. https://doi.org/10.1016/j.nlm.2013.09.007.

69. Trask, Sydney, Nicole C. Ferrara, Kevin Grisales, and Fred J. Helmstetter. "Optogenetic Inhibition of Either the Anterior or Posterior Retrosplenial Cortex Disrupts Retrieval of a Trace, but Not Delay, Fear Memory." *Neurobiology of Learning and Memory* 185 (November 2021): 107530. https://doi.org/10.1016/j.nlm.2021.107530.

70. Han, C. J., Colm M. O'Tuathaigh, Laurent van Trigt, Jennifer J. Quinn, Michael S. Fanselow, Raymond Mongeau, Christof Koch, and David J. Anderson. "Trace but Not Delay Fear Conditioning Requires Attention and the Anterior Cingulate Cortex." *Proceedings of the National Academy of Sciences of the United States of America* 100, no. 22 (October 28, 2003): 13087–92. https://doi.org/10.1073/pnas.2132313100.

71. Cowansage, Kiriana Kater, Tristan Shuman, Blythe Christine Dillingham, Allene Chang, Peyman Golshani, and Mark Mayford. "Direct Reactivation of a Coherent Neocortical Memory of Context." *Neuron* 84, no. 2 (October 22, 2014): 432–41. https://doi.org/10.1016/j.neuron.2014.09.022.

72. Catlow, Briony J., Shijie Song, Daniel A. Paredes, Cheryl L. Kirstein, and Juan Sanchez-Ramos. "Effects of Psilocybin on Hippocampal Neurogenesis and Extinction of Trace Fear Conditioning." *Experimental Brain Research* 228, no. 4 (August 1, 2013): 481–91. https://doi.org/10.1007/s00221-013-3579-0.

73. Williams, Alex H., Tony Hyun Kim, Forea Wang, Saurabh Vyas, Stephen I. Ryu, Krishna V. Shenoy, Mark Schnitzer, Tamara G. Kolda, and Surya Ganguli. "Unsupervised Discovery of Demixed, Low-Dimensional Neural Dynamics across Multiple Timescales through Tensor Component Analysis." *Neuron* 98, no. 6 (June 27, 2018): 1099-1115.e8. https://doi.org/10.1016/j.neuron.2018.05.015.

74. Pennington, Zachary T., Zhe Dong, Yu Feng, Lauren M. Vetere, Lucia Page-Harley, Tristan Shuman, and Denise J. Cai. "ezTrack: An Open-Source Video Analysis Pipeline for the Investigation of Animal Behavior." *Scientific Reports* 9, no. 1 (December 27, 2019): 19979. https://doi.org/10.1038/s41598-019-56408-9.

75. Vohryzek, Jakub, Joana Cabral, Louis-David Lord, Henrique M. Fernandes, Leor Roseman, David J. Nutt, Robin L. Carhart-Harris, Gustavo Deco, and Morten L. Kringelbach. "Brain Dynamics Predictive of Response to Psilocybin for Treatment-Resistant Depression." *Brain Communications* 6, no. 2 (2024): fcae049. https://doi.org/10.1093/braincomms/fcae049.

76. Ekins, Tyler G, Isla Brooks, Sameer Kailasa, Chloe Rybicki-Kler, Izabela Jedrasiak-Cape, Ethan Donoho, George A. Mashour, Jason Rech, and Omar J Ahmed. "Cellular Rules Underlying Psychedelic Control of Prefrontal Pyramidal Neurons." Preprint. Neuroscience, October 23, 2023. https://doi.org/10.1101/2023.10.20.563334.

77. Effinger, D. P., S. G. Quadir, M. C. Ramage, M. G. Cone, and M. A. Herman. "Sex-Specific Effects of Psychedelic Drug Exposure on Central Amygdala Reactivity and Behavioral Responding." *Translational Psychiatry* 13, no. 1 (April 8, 2023): 119. https://doi.org/10.1038/s41398-023-02414-5.

78. Tomé, Douglas Feitosa, Ying Zhang, Tomomi Aida, Olivia Mosto, Yifeng Lu, Mandy Chen, Sadra Sadeh, Dheeraj S. Roy, and Claudia Clopath. "Dynamic and Selective Engrams Emerge with Memory Consolidation." *Nature Neuroscience*, January 19, 2024, 1–12. https://doi.org/10.1038/s41593-023-01551-w.

79. Kwan, Alex C., David E. Olson, Katrin H. Preller, and Bryan L. Roth. "The Neural Basis of Psychedelic Action." *Nature Neuroscience* 25, no. 11 (November 2022): 1407–19. https://doi.org/10.1038/s41593-022-01177-4.

80. Park, Youngmin, and Maria N. Geffen. "A Circuit Model of Auditory Cortex." *PLOS Computational Biology* 16, no. 7 (July 27, 2020): e1008016. https://doi.org/10.1371/journal.pcbi.1008016.

Supplementary Materials.
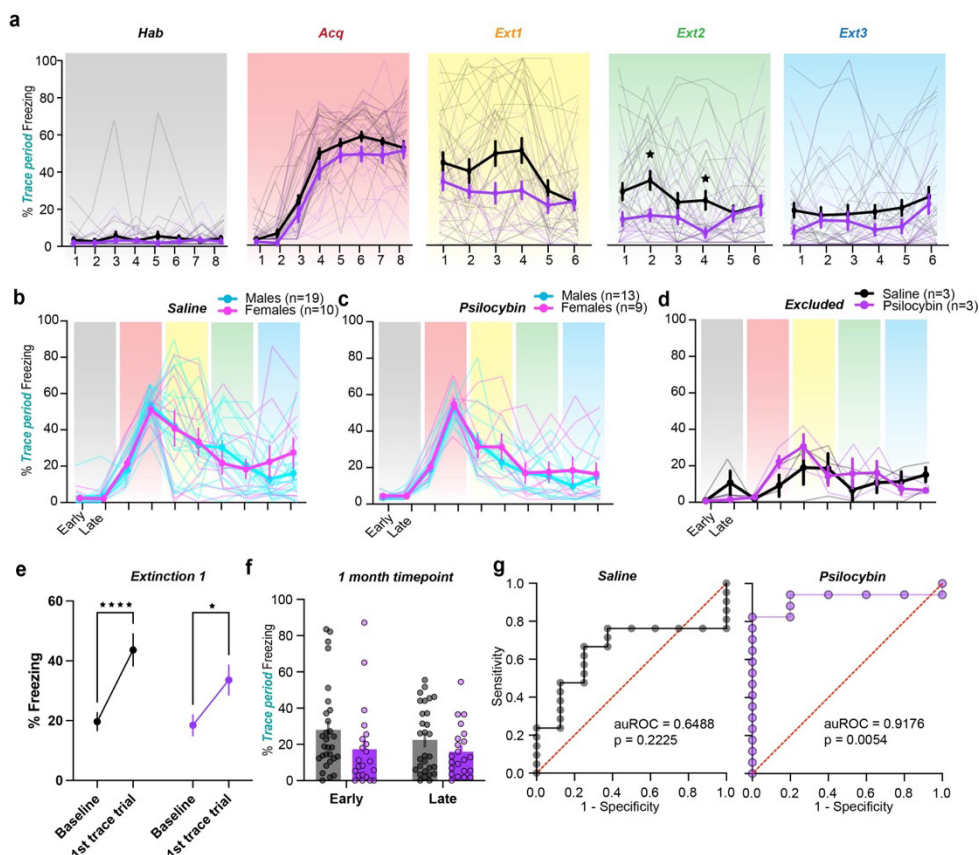
Supplementary Figure 1 │ Effects of psilocybin on trace fear extinction in males and females.
a. Trial by trial freezing of saline- and psilocybin-administered mice. Two-Way RM ANOVA with Sidak multiple comparisons correction. (Supp. Table 1, rows 102-106) **b.** Half-session freezing by sex of saline-administered animals. Two-Way RM ANOVA with Sidak multiple comparisons correction. (Supp. Table 1, row 107) **c.** Same as B) in psilocybin-administered animals. Two-Way RM ANOVA with Sidak multiple comparisons correction. (Supp. Table 1, row 108) **d.** Half-session freezing by treatment of excluded animals. Two-Way RM ANOVA with Sidak multiple comparisons correction. (Supp. Table 1, row 109) **e.** Percent freezing during the baseline vs. trace period during Extinction 1. Two-Way RM ANOVA with Sidak multiple comparisons correction. (Supp. Table 1, row 110) **f.** Percent trace-period freezing in early and late periods during an Extinction session 1 month after Extinction 3. Two-Way RM ANOVA with Sidak multiple comparisons correction. (Supp. Table 1, row 111) **g.** ROC curves from logistic regression predicting RE or SE status based on % time freezing during the first half of *Extinction 1* during acute drug treatment in saline-administered mice (left) and psilocybin administered mice (right). Right: ROC curve from logistic regression. (Supp. Table 1, rows 12, 14) * $p \leq 0.05$, ** $p < 0.01$, *** $p < 0.001$, **** $p < 0.0001$.
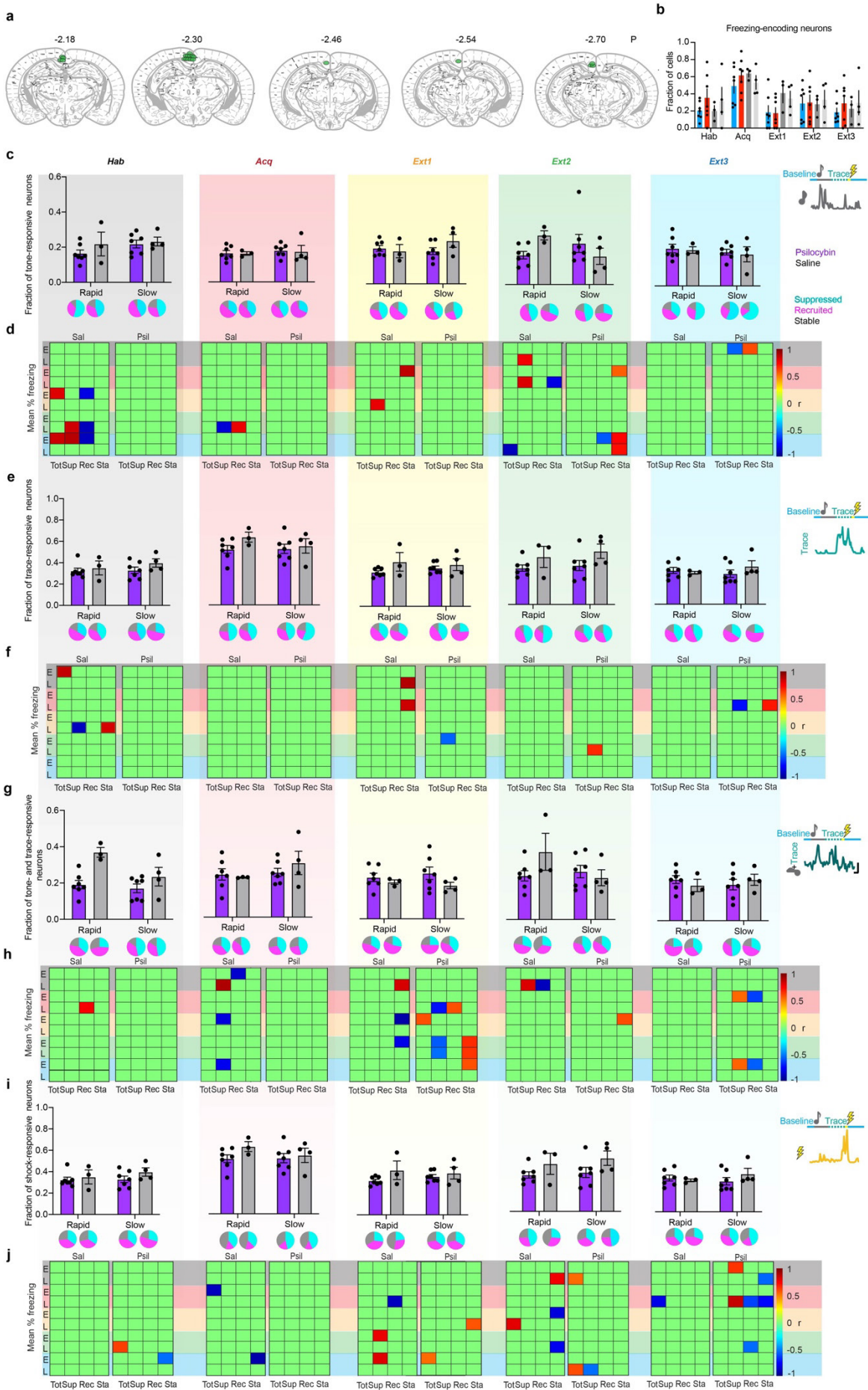
Supplementary Figure 2 *continued* | **All RSC cells recorded.**

a. Center and bottom of implant tracts of all included mice from anterior (left) to posterior (right) granular RSC. **b.** Fraction of freezing encoding neurons on each day. Two-way RM ANOVA. (Supp. Table 1, row 112) **c.** Mean fraction of tone-responsive neurons on each day. Insets are proportions of neurons with suppressed, recruited, and stable responses. Two-Way ANOVA. (Supp. Table 1, rows 113-117) **d.** Heatmaps displaying significant correlations (Pearson's rho) between proportions of total (Tot), suppressed (Sup), recruited (Rec), and stable (Sta) tone-responsive neurons on each day and % freezing during the early (E) and late (L) halves of each session (black rows = Hab freezing and black columns = fractions of neurons during Hab, red = Acq, yellow = Ext1, green = Ext2, blue = Ext3). **e,g,i.** Same as C for trace-, tone-and-trace, and shock-responsive neurons. Two-Way ANOVA. (Supp. Table 1, rows 118-132) **f,h,j.** Same as D for trace-, tone-and-trace, and shock-responsive neurons. Data are represented as mean ± SEM. * p ≤ 0.05, ** p < 0.01, *** p < 0.001, **** p < 0.0001.
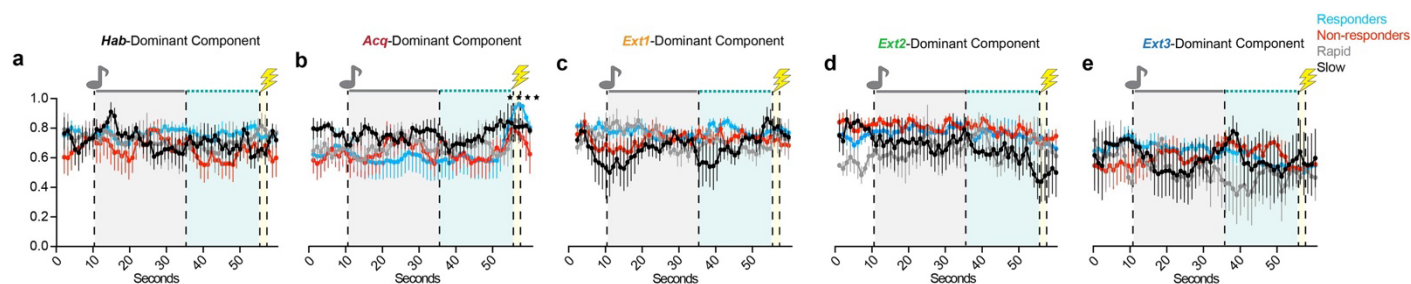
Supplementary Figure 3 | **TCA factors reveal RSC dynamics modulated by session.**

a. Normalized temporal factor weights by group of the Habituation-dominant component. Two-Way RM ANOVA. (Supp. Table 1, row 133) **b.** Same as A) for the Acquisition-dominant component. Two-Way RM ANOVA. (Supp. Table 1, row 134) **c.** Same as A) for the Extinction 1-dominant component. Two-Way RM ANOVA. (Supp. Table 1, row 135) **d.** Same as A) for the Extinction 2-dominant component. Two-Way RM ANOVA. (Supp. Table 1, row 136) **e.** Same as A) for the Extinction 3-dominant component. Two-Way RM ANOVA. (Supp. Table 1, row 137) Data are represented as mean ± SEM. * p ≤ 0.05, ** p < 0.01, *** p < 0.001, **** p < 0.0001.
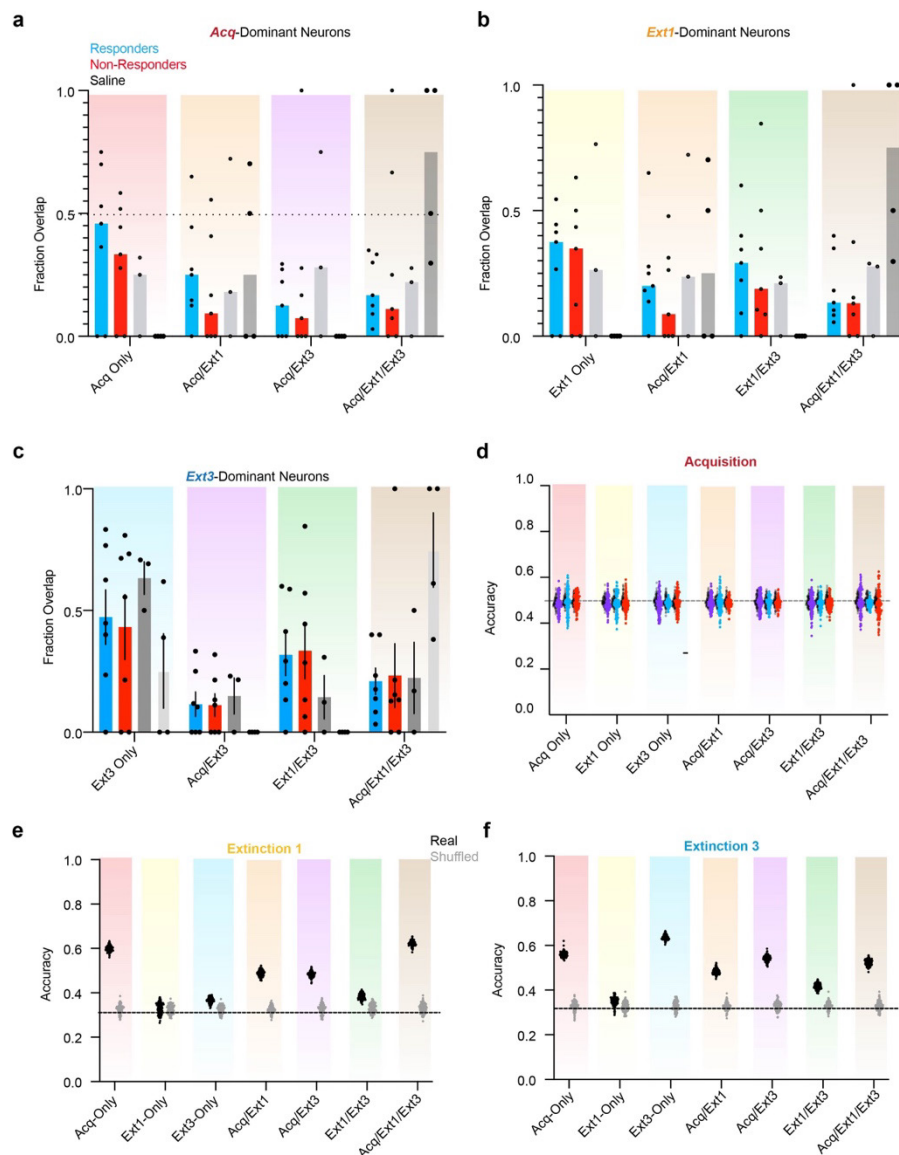
Supplementary Figure 4 | Psilocybin bidirectionally modulates neural ensembles driving RSC dynamics during TFC in responders.

a. Overlaps of ensembles within individual animals comprising the mean values in Fig. 4B top. Bars are median. **b.** Same as A for Fig. 4B middle. **c.** Same as A for Fig. 4B middle. **d.** Fisher decoder performance on Acquisition activity in functionally defined ensembles of cells to distinguish responders vs. non-responders (purple), responders vs. rapid saline (blue around grey), and non-responders vs. rapid saline (red around grey). 100 iterations for each comparison. Shuffled values are behind real values. **e.** Three-way Fisher decoder performance classifying responders vs. non-responders vs. rapidly extinguishing saline mice trained on activity during Extinction 1. **f.** Same as E for Extinction 3 activity.
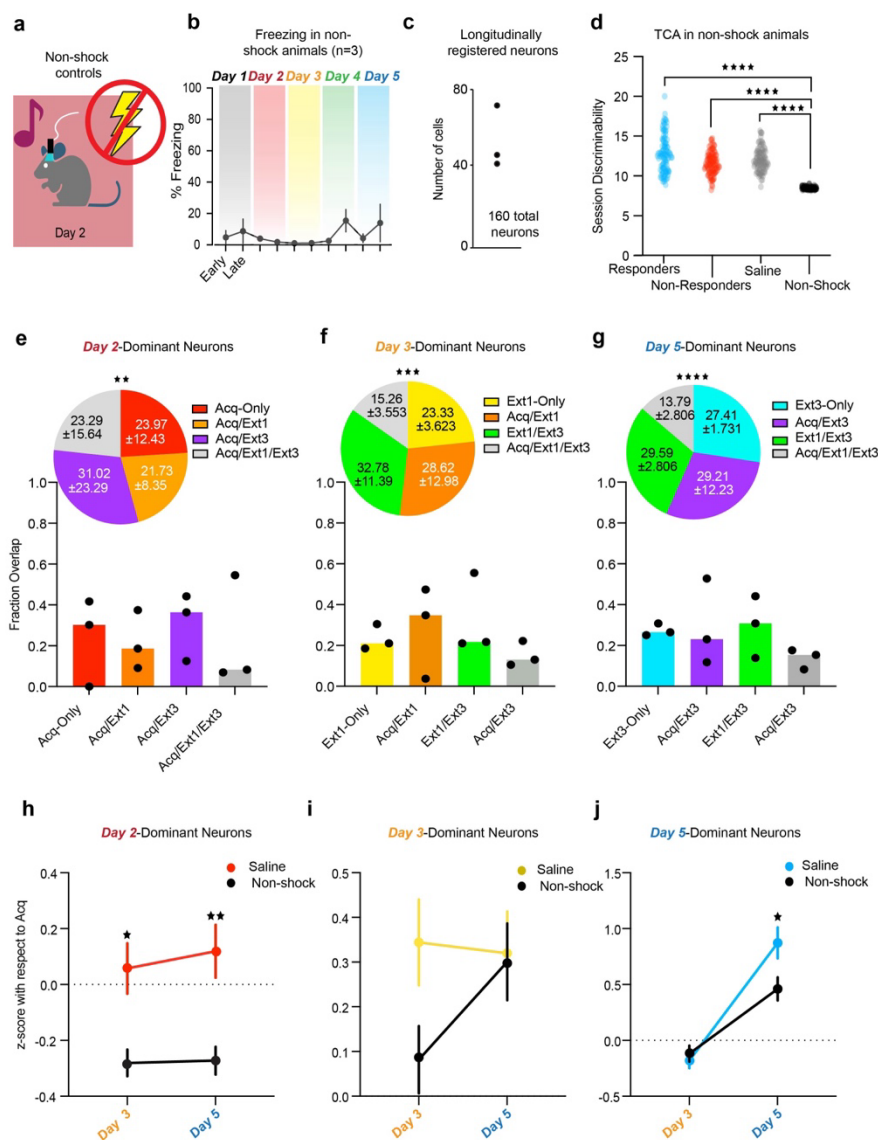
Supplementary Figure 5 │ Non-shock controls do not exhibit conditioning-associated dynamics.
a. Schematic of non-shock protocol. 3 Miniscope implanted mice underwent identical 5 day paradigm to all other mice, with the exception that they received no shock during Acquisition or drug treatment. **b.** Half-session freezing in non-shock mice. (Supp. Table 1, row 138). **c.** Number of longitudinally registered neurons in non-shock mice. **d.** Sum of session discriminability index. Because roughly half the number of neurons were recorded in non-shock mice as in the other two groups, pooled tensors from psilocybin responders, non-responders, and saline mice were subsampled to a different, random set of 160 neurons in each of 100 iterations of TCA. One-Way ANOVA. (Supp. Table 1, rows 139). **e.** Overlap of the *Day 2*-dominant ensemble with *Day 3*- and *Day 5*-dominant ensembles in non-shock mice. Bar graphs display the median fraction overlaps. Dots are individual animals. Insets are pie charts displaying total overlap. Stars indicate comparison to saline distribution. Chi-square. (Supp. Table 1, rows 140) **f.** Same as E for the *Day 3*-dominant ensemble. Chi-square. (Supp. Table 1, rows 141). **g.** Same as F for the *Day 5*-dominant ensemble. Chi-square. (Supp. Table 1, rows 142) **h.** Average z-score with respect to *Day 2* of *Day 2*-dominant ensemble during *Day 3* and *5* in non-shock mice (black) compared to conditioned, saline-administered mice. Two-Way RM ANOVA. (Supp. Table 1, rows 143). **I.** Same as H for the *Day 3*-dominant ensemble. (Supp. Table 1, rows 144). **j.** Same as H for the *Day 5*-dominant ensemble. (Supp. Table 1, rows 145). Data are represented as mean ± SEM. * p ≤ 0.05, ** p < 0.01, *** p < 0.001, **** p < 0.0001.
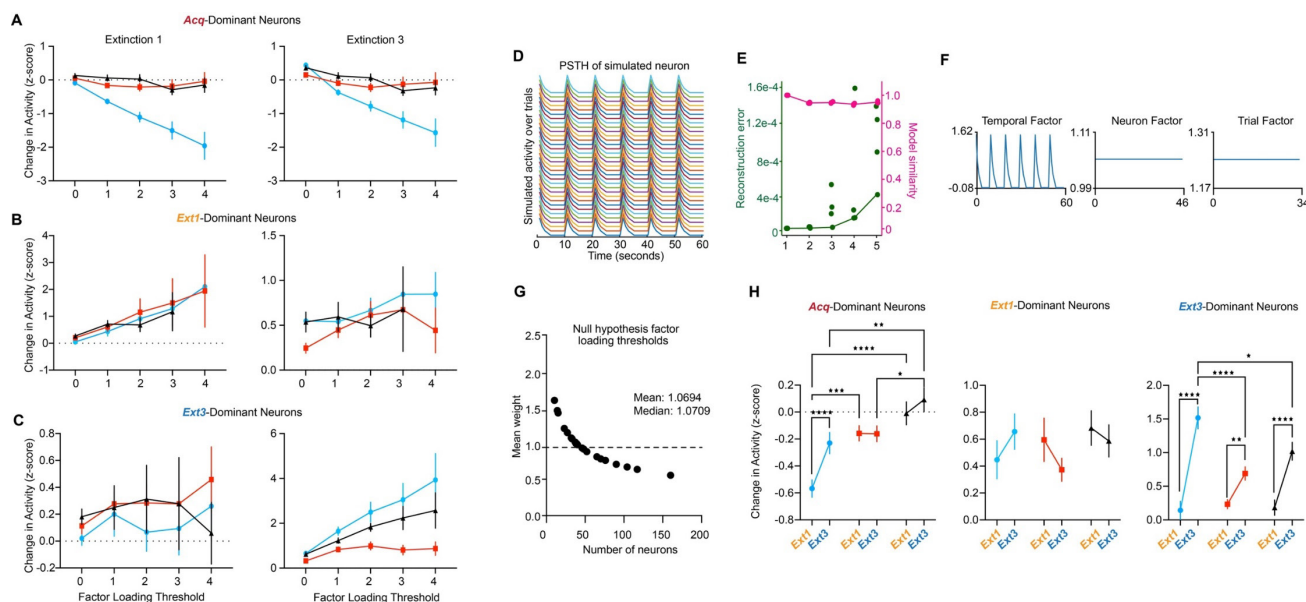
Supplementary Figure 6 | Results are robust to changes in factor loading thresholds.
a. Change in activity in mean ± SEM from *Acquisition* in *Acq*-dominant neurons as a function of factor loading thresholds varying between *w*=0-4 during *Extinction 1* (left) and *Extinction 3* (right). **b.** Same as A) for *Ext1*-dominant neurons. **c.** Same as A) for *Ext3*-dominant neurons. **d.** PSTH of an example simulated neuron to determine the null hypothesis factor loading threshold. Tensors of t x c x T size, where c is the number of neurons recorded in a given animal, were created with identically behaving neurons to determine the factor loading threshold in a hypothetical population in which each neuron equally contributes to dynamics, or the null hypothesis factor loading threshold for that animal. **e.** Reconstruction error and model similarity of varying model ranks for populations of identical neurons. A model of rank 1 yields 0 error in this case. **f.** Representative rank 1 TCA of a simulated dataset with n=46 neurons, the median number of neurons recorded in this study. Because variances across trials and neurons were clamped at 0, only the temporal factor varies. **g.** Data in Fig. 4A plotted as a function of number of neurons recorded. Mean weight of neuron factors across 100 iterations of TCA at the number of cells recorded in each animal. **h.** Change in activity in mean ± SEM from *Acquisition* during *Extinction 1* and *3* in *Acq*-dominant (left), *Ext1*-dominant (middle), and *Ext3*-dominant (right) using ensembles determined with the null hypothesis factor loading for each animal. Two-way RM ANOVA. (Supp. Table 1, rows 88-90) . * $p \leq 0.05$, ** $p < 0.01$, *** $p < 0.001$, **** $p < 0.0001$.
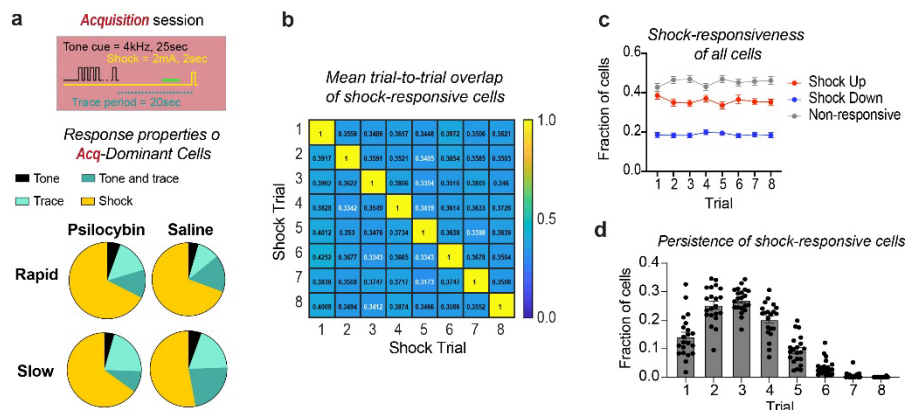
Supplementary Figure 7 | Shock-responsive neurons are unstable in the RSC.

a. Average proportions of Acq-dominant neurons in each group that were upregulated in response to shock, trace, tone, or tone-and-trace. **b.** Heatmap of the average fraction of overlap in shock-up neurons between each trial of Acquisition. Average overlap between trials ranges from 30-45%. **c.** Fractions of shock-up, shock-down, or shock-nonresponsive neurons across all 21 mice on each trial of acquisition, determined by permutation test. **d.** Persistence of the response properties of shock-up neurons over the session. Each point y is the fraction of neurons upregulated in response to the shock for x number of trials. Data are represented as mean ± SEM over all 21 mice.

Row	Figure	Statistical Model	Variable	Degrees of Freedom (DFn, DFd)	Parameter(s)	Paramter value	p-value	Multiple comparisons? (Sidak test)	p-value	n per group
1	Fig. 1B, panel 1	Two Way RM-ANOVA	Treatment			0.2838	0.1969			29 sal, 22 psil
			Time			1.712	0.1969			
			Interaction	(1,49)	F-statistic	1.715	0.9741			
2	Fig. 1B, panel 2	Two Way RM-ANOVA	Treatment			0.6344	0.4296			29 sal, 22 psil
			Time			557.5	<0.0001			
			Interaction	(1,49)	F-statistic	0.04144	0.8395			
3	Fig. 1B, panel 3	Two Way RM-ANOVA	Treatment			2.863	0.565			29 sal, 22 psil
			Time			9.184	0.0039			
			Interaction	(1,49)	F-statistic	0.3357	0.097			
4	Fig. 1B, panel 4	Two Way RM-ANOVA	Treatment			5.072	0.0288			29 sal, 22 psil
			Time			8.207	0.0061			
			Interaction	(1,49)	F-statistic	5.236	0.0265	Sidak: Early, Late	Early: 0.0093, Late: 0.3329	
5	Fig. 1B, panel 5	Two Way RM-ANOVA	Treatment			1.773	0.6977			29 sal, 22 psil
			Time			2.326	0.1337			
			Interaction	(1,49)	F-statistic	0.1527	0.1891			
6	Fig. 1C	Mann-Whitney	Treatment		Mann-Whitney U	235	0.1116			29 sal, 22 psil
7	Fig. 1D, panel 1	Two Way RM-ANOVA	Treatment	(3,47)		0.7305	0.539			5-21 mice
			Time	(1,47)		0.2511	0.6187			
			Interaction	(3,47)	F-statistic	0.5344	0.661			
8	Fig. 1D, panel 2	Two Way RM-ANOVA	Treatment	(3,47)		0.7676	0.518			5-21 mice
			Time	(1,47)		482	<0.0001			
			Interaction	(3,47)	F-statistic	4.265	0.0096			
9	Fig. 1D, panel 3	Two Way RM-ANOVA	Treatment	(3,47)		2.793	0.0506			5-21 mice
			Time	(1,47)		7.015	0.011			
			Interaction	(3,47)	F-statistic	0.9362	0.4307			
10	Fig. 1D, panel 4	Two Way RM-ANOVA	Treatment	(3,47)		5.415	0.0028	Sidak: Early, Late	Early: Sal RE vs. Psil RE 0.0114; Sal SE vs. Psil SE 0.0059 Late: Sal RE vs. Psil SE 0.0190; Psil RE vs. Sal SE: 0.008; Psil RE vs. Psil SE 0.0337;	5-21 mice
			Time	(1,47)		3.069	0.0863			
			Interaction	(3,47)	F-statistic	2.948	0.0423			
11	Fig. 1D, panel 5	Two Way RM-ANOVA	Treatment	(3,47)		29.27	0.0001	Sidak: Early, Late	Early: Sal RE vs. Sal SE <0.0001; Sal RE vs. Psil SE 0.0174; Psil RE vs. Sal SE <0.0001; Psil RE vs. Psil SE <0.0039; Late: Sal RE vs. Sal SE <0.0001; Sal RE vs. Psil SE 0.0001; Psil RE vs. Sal SE <0.0001; Psil RE vs. Psil SE <0.0001	5-21 mice
			Time	(1,47)		7.377	0.0092			
			Interaction	(3,47)	F-statistic	2.606	0.2058			
12	Fig. 1F, panel 1	Logistic regression	Extinction rate class		beta0/log likelihood/auROC	1.458±0.7874 / 0.5949 / 0.6488	0.4411/ 0.4405 / 0.2225			5-21 mice
13	Fig. 1F, panel 2	Two Way RM-ANOVA	Group	(9, 243)		17.38	0.0066	Sidak: Session half	Ext3 late: 0.0021	7-18 mice
			Time	(2.967, 80.11)		33.75	<0.0001			
			Interaction	(1,27)	F-statistic	17.38	<0.0001			
14	Fig. 1G, panel 1	Logistic regression	Extinction rate class		beta0/log likelihood/ auROC	3.772±1.487 / 6.477 / 0.9251	0.0392 / 0.0109 / 0.0054			5-21 mice
15	Fig. 1G, panel 2	Two Way RM-ANOVA	Group	(9, 243)		16.97	0.0005	Sidak: Session half	Ext1 late: 0.0235, Ext2 late: 0.006, Ext3 late: 0.0143	7-18 mice
			Time	(2.967, 80.11)		39.91	<0.0001			
			Interaction	(1,27)	F-statistic	6.473	<0.0001			
16	Fig. 2F, panel 1	Two Way RM-ANOVA	Group	(3,17)		2.014	0.1502			3-7 mice
			Time	(7, 119)		1.685	0.1191			
			Interaction	(21, 119)	F-statistic	1	0.7516			
17	Fig. 2F, panel 2	Two Way RM-ANOVA	Group	(3,17)		0.6155	0.6143			3-7 mice
			Time	(7, 119)		23.36	<0.0001			
			Interaction	(21, 119)	F-statistic	0.8446	0.6605			
18	Fig. 2F, panel 3	Two Way RM-ANOVA	Group	(3, 17)		0.4326	0.7324			3-7 mice
			Time	(5,85)		1.404	0.2312			
			Interaction	(15, 85)	F-statistic	0.6765	0.8004			
19	Fig. 2F, panel 4	Two Way RM-ANOVA	Group	(3, 17)		1,162	0.353			3-7 mice
			Time	(5,85)		1.462	0.2107			
			Interaction	(15, 85)	F-statistic	0.6521	0.8229			
20	Fig. 2F, panel 5	Two Way RM-ANOVA	Group	(3, 17)		7.78	0.0017	Sidak: Trials	Trial 2: Res vs. Non 0.0479; Trial 4:Res vs. Non 0.0181	3-7 mice
			Time	(5,85)		0.9564	0.4493			
			Interaction	(15, 85)	F-statistic	0.5976	0.8691			
21	Fig. 2F, panel 6	Unpaired t-test	Group	(2, 18)	F-statistic	1.254	0.3615			3-7 mice
22	Fig. 2J	Two Way RM ANOVA	Group	(3, 17)		0.2566	0.4897			
			Time	(4,68)		0.6486	0.6298			
			Interaction	(12, 68)	F-statistic	0.9656	0.4897			
			Group	(3, 17)		0.04281	0.9878			

Row	Figure	Statistical Model	Variable	Degrees of Freedom (DFn, DFd)	Parameter(s)	Paramter value	p-value	Multiple comparisons? (Sidak test)	p-value	n per group
23	Fig. 2K	Two Way RM ANOVA	Time	(4,68)		5.506	0.0007			
			Interaction	(12, 68)	F-statistic	1.106	0.3109			3-7 mice
24	Fig. 2L	Two Way RM ANOVA	Group	(3, 17)		1.461	0.2606			
			Time	(4,68)		0.9682	0.4308			
			Interaction	(12, 68)	F-statistic	0.7331	0.7144			3-7 mice
25	Fig. 2M	Two Way RM ANOVA	Group	(3, 17)		0.2848	0.8357			
			Time	(4,68)		50.48	<0.0001			
			Interaction	(12, 68)	F-statistic	1.534	0.1335			3-7 mice
26	Fig. 2N	Two Way RM ANOVA	Group	(3, 17)		0.2464	0.979			
			Time	(4,68)		110.3	<0.0001			
			Interaction	(12, 68)	F-statistic	0.3381	0.8626			3-7 mice
27	Fig. 2O	Two Way RM ANOVA	Group	(3, 17)		0.7136	0.5573			
			Time	(4,68)		154.6	<0.0001			
			Interaction	(12, 68)	F-statistic	0.6438	0.7974			3-7 mice
28	Fig. 2P	Two Way RM ANOVA	Group	(3, 17)		0.435	0.7308			
			Time	(2.679, 45.54)		13.15	<0.0001			
			Interaction	(12, 68)	F-statistic	1.213	0.2808			3-7 mice
29	Fig. 3A, panel 1	Two Way ANOVA	Treatment	(1, 17)		1.779	0.1998			
			Extinction class	(1,17)		0.4785	0.4984			
			Interaction	(1,17)	F-statistic	0.5428	0.4713			3-7 mice
30	Fig. 3A, panel 2	Two Way ANOVA	Treatment	(1, 17)		0.1064	0.7482			
			Extinction class	(1,17)		0.4287	0.5214			
			Interaction	(1,17)	F-statistic	3.734	0.0702			3-7 mice
31	Fig. 3A, panel 3	Two Way ANOVA	Treatment	(1, 17)		48.57	<0.0001	Sidak: Psil vs. Sal	Rapid: <0.0001; Slow: 0.0004	
			Extinction class	(1,17)		0.403	0.534			
			Interaction	(1,17)	F-statistic	1.219	0.285			3-7 mice
32	Fig. 3A, panel 4	Two Way ANOVA	Treatment	(1, 17)		1.432	0.2479			
			Extinction class	(1,17)		0.4266	0.5224			
			Interaction	(1,17)	F-statistic	4.623	0.0462	Sidak: Psil vs. Sal	Slow psil v. slow sal: 0.0464	3-7 mice
33	Fig. 3A, panel 5	Two Way ANOVA	Treatment	(1, 17)		1.148	0.3473			
			Extinction class	(1,17)		1.616	0.2207			
			Interaction	(1,17)	F-statistic	1.148	0.299			3-7 mice
34	Fig. 3B, panel 1	Two Way ANOVA	Treatment	(1, 17)		3.335	0.0854			
			Extinction class	(1,17)		0.4659	0.5041			
			Interaction	(1,17)	F-statistic	1	0.2761			3-7 mice
35	Fig. 3B, panel 2	Two Way ANOVA	Treatment	(1, 17)		0.04985	0.826			
			Extinction class	(1,17)		3.258	0.0888			
			Interaction	(1,17)	F-statistic	0.6745	0.6745			3-7 mice
36	Fig. 3B, panel 3	Two Way ANOVA	Treatment	(1, 17)		14.97	0.0012	sidak: psil v sal	rapid: 0.1184; slow: 0.0049	
			Extinction class	(1,17)		0.07179	0.792			
			Interaction	(1,17)	F-statistic	0.8108	0.3805			3-7 mice
37	Fig. 3B, panel 4	Two Way ANOVA	Treatment	(1, 17)		0	0.7698			
			Extinction class	(1,17)		0.685	0.4193			
			Interaction	(1,17)	F-statistic	0.0884	0.8432			3-7 mice
38	Fig. 3B, panel 5	Two Way ANOVA	Treatment	(1, 17)		0.002783	0.9585			
			Extinction class	(1,17)		3.41	0.0823			
			Interaction	(1,17)	F-statistic	3.41	0.0823			3-7 mice
39	Fig. 3E, panel 1	Two Way ANOVA	Treatment	(1, 17)		0.1006	755			
			Extinction class	(1,17)		0.8545	0.3682			
			Interaction	(1,17)	F-statistic	0.6187	0.4423			3-7 mice
40	Fig. 3E, panel 2	Two Way ANOVA	Treatment	(1, 17)		0.2706	0.054			
			Extinction class	(1,17)		2.857	0.1092			
			Interaction	(1,17)	F-statistic	4.285	0.6097			3-7 mice
41	Fig. 3E, panel 3	Two Way ANOVA	Treatment	(1, 17)		20.69	0.0003			
			Extinction class	(1,17)		10.27	0.0052			
			Interaction	(1,17)	F-statistic	9.196	0.0075	Sidak	rapid sal v psil: 0.0002 sal rapid v slow: 0.0028	3-7 mice
42	Fig. 3E, panel 4	Two Way ANOVA	Treatment	(1, 17)		0.08971	0.7682			
			Extinction class	(1,17)		0.1562	0.6976			
			Interaction	(1,17)	F-statistic	0.09206	0.7653			3-7 mice
43	Fig. 3E, panel 5	Two Way ANOVA	Treatment	(1, 17)		0.2325	0.6358			
			Extinction class	(1,17)		7.921	0.0119	Sidak: psil	rapid v slow: 0.0136	
			Interaction	(1,17)	F-statistic	0.5108	0.6358			3-7 mice
44	Fig. 3FF panel 1	Two Way ANOVA	Treatment	(1, 17)		0.06716	0.1367			
			Extinction class	(1,17)		0.01831	0.8939			
			Interaction	(1,17)	F-statistic	2.401	0.7516			3-7 mice
45	Fig. 3F, panel 2	Two Way ANOVA	Treatment	(1, 17)		0.6654	0.4295			
			Extinction class	(1,17)		0.1733	0.6824			
			Interaction	(1,17)	F-statistic	6.323	0.0223			3-7 mice
46	Fig. 3F, panel 3	Two Way ANOVA	Treatment	(1, 17)		43.19	<0.0001	Sidak: rapid v slow	sal; .0081; psil; <0.0001	
			Extinction class	(1,17)		1.651	0.2161			
			Interaction	(1,17)	F-statistic	4.437	0.0503			3-7 mice
47	Fig. 3F, panel 4	Two Way ANOVA	Treatment	(1, 17)		1	0.527			
			Extinction class	(1,17)		0.2496	0.6238			
			Interaction	(1,17)	F-statistic	0.4172	0.4045			3-7 mice
			Treatment	(1, 17)		0.6719	0.4237			

Row	Figure	Statistical Model	Variable	Degrees of Freedom (DFn, DFd)	Parameter(s)	Paramter value	p-value	Multiple comparisons? (Sidak test)	p-value	n per group
48	Fig. 3F, panel 5	Two Way ANOVA	Extinction class	(1,17)		0.458	0.5077			
			Interaction	(1,17)	F-statistic	1.523	0.234			3-7 mice
49	Fig. 3G, top	Linear regression	PC distance during ext3 x freezing late ext3, psil	(1,12)	F-statistic/Beta 0/R2	16.61 / -191.8±47.07 / 0.5805	0.0015			14 mice
50	Fig. 3G, bottom	Linear regression	PC distance during ext3 x freezing late ext3, sal	(1,5)	F-statistic/Beta 0/R2	.6275 -100.5±126.9 / 0.1115	0.4642			7 mice
51	Fig. 4B, panel 1	Two Way RM ANOVA	Sex	(3, 17)		0.4119	0.7465			
			Time	(33, 561)		14.28	<0.0001			
			Interaction	(99, 561)	F-statistic	0.7388	0.9684			7 mice
52	Fig. 4B, panel 2	Two Way RM ANOVA	Sex	(3, 17)		6.775	0.0033			
			Time	(33, 561)		11.96	<0.0001			
			Interaction	(99, 561)	F-statistic	1.27	0.0515			7 mice
53	Fig. 4B, panel 3	Two Way RM ANOVA	Sex	(3, 17)		1.71	0.2029			
			Time	(33, 561)		9.227	<0.0001			
			Interaction	(99, 561)	F-statistic	1.71	0.3224			7 mice
54	Fig. 4B, panel 4	Two Way RM ANOVA	Sex	(3, 17)		1.46	0.2609			
			Time	(33, 561)		19.95	<0.0001			
			Interaction	(99, 561)	F-statistic	1.125	0.2092			7 mice
55	Fig. 34, panel 5	Two Way RM ANOVA	Sex	(3, 17)		0.5065	0.583			
			Time	(33, 561)		17.3	<0.0001			
			Interaction	(99, 561)	F-statistic	1.333	0.025			7 mice
56	Fig. 4C, solid	Ordinary One-Way ANOVA	Group	(3,17)	F-statistic	0.3857	1			7 mice
57	Fig. 4C, checkered	Ordinary One-Way ANOVA	Group	(3,17)	F-statistic	0.7163	0.5558			7 mice
58	Fig. 4D	Multiple unpaired t-tests	Dateset (real vs. shuffled)	198	t-statistic	144.1; 115.9; 25.21; 38.53	<0.0001; <0.0001; <0.0001; <0.0001			100 iterations
59	Fig. 4E - data for	Multiple linear regression	Component trial factor weight X trial by trial freezing		F-statistic/R2	for each animal (res, nonres, rapid, slow): 24.2871 0.8126 7.262 0.5646 10.0595 0.6424 2.7637 0.3304 5.1204 0.4776 6.6871 0.5442 4.7136 0.457 8.9874 0.6161 5.2324 0.483 3.8343 0.4064 5.7258 0.5056 1.7432 0.2374 8.4946 0.6027 4.3268 0.4359 3.2644 0.3683 5.7293 0.5057 4.2004 0.4286 3.3388 0.3735 3.1072 0.3569 2.0108 0.2642 2.4635 0.3055	for each animal (res, nonres, sal): 0 0 0.0002 0.0016 0 0.009 0.0376 0.0009 0.0019 0.1575 0.0003 0.0001 0.003 0.0048 0.0191 0.0009 0.0057 0.0235 0.1079 0.0571 0.0172			21 mice
60	Fig. 4E	One sample t-test	Median correlation between component trial factor weight X trial by trial freezing > 0	6; 6; 2; 3	t-statistic	res: 29.481/ non-res: 9.638/ rapid: 13.05; slow = 10.92	res: <0.0001; non-res: <0.0001; rapid; 0.0083; slow;0.0081			
61	Fig. 4F, column 1	Linear regression	Strength of component in session X extinction rate	(1,19)	F-statistic/Beta 0/R2	H: 0.6973 / -0.07817 / 0.03540; A: 0.4962, / 0.05690 / 0.02545; E1 0.6020 / 0.05855 / 0.03071; E2: 0.1427/ 0.01963 / 0.007452; E3: 0.4347 / 0.04096 / 0.02237	H: 0.4141, A: 0.4897, E1: 0.4474, E2: 0.7098, E3 0.5176			21 mice
62	Fig. 4F, column 2	Linear regression	Strength of component in session X extinction rate	(1,19)	F-statistic/Beta 0/R2	H: 0.2515/ 0.04533 / 0.01306; A: 2.692 / -0.1296 / 0.1241; E1 -0.02112 / -0.02112 / 0.002113; E2: 0.1427/ 0.0755 / 0.05979; E3: 0.4347 / 0.09385 / 0.1285	H: 0.6218, A: 0.1173, E1: 0.8431, E2: 0.2854, E3 0.1106			21 mice
63	Fig. 4F, column 3	Linear regression	Strength of component in session X extinction rate	(1,19)	F-statistic/Beta 0/R2	H: 0.1744 / -0.03684/ 0.009095; A: 0.4962, / -0.02452 / 0.005961; E1 2.394 / -0.1309 / 0.1119; E2: 0.2255/ -0.0564 / 0.01173; E3: 0.04184 /-0.02214 / 0.002197	H: 0.6809, A: 0.7394, E1: 0.1383, E2: 0.6403, E3 0.8401			21 mice

Row	Figure	Statistical Model	Variable	Degrees of Freedom (DFn, DFd)	Parameter(s)	Paramter value	p-value	Multiple comparisons? (Sidak test)	p-value	n per group
64	Fig. 4F, column 4	Linear regression	Strength of component in session X extinction rate	(1,19)	F-statistic/Beta 0/R2	H: 2.029 / 0.1275 / 0.0965; A: 0.03238, / -0.01209 0.001701; E1 0.006821 / -0.008477 / 0.0003589; E2: 5.533/ -0.1994 / 0.2255; E3: 0.2794 / 0.03526 / 0.01449	H: 0.1705, A: 0.8591, E1: 0.935, E2: 0.0296, E3 0.6032			21 mice
65	Fig. 4F, column 5	Linear regression	Strength of component in session X extinction rate	(1,19)	F-statistic/Beta 0/R2	H: 0.06392 / 0.02579 / 0.003353; A: 2.43, / 0.07323 / 0.1134; E1 0.218 / 0.05245 / 0.01134; E2: 0.9223/ 0.0414 / 0.0463; E3: 10.8 /-0.2158 / 0.3624	H: 0.8031, A: 0.1355, E1: 0.6459, E2: 0.3489, E3 0.0039			21 mice
66	Fig. 4G	Linear regression	Component strength X extinction rate	(1,19)	F-statistic/Beta 0/R2	11.74 / -1.579±0.4607 / 0.3820	0.0028			21 mice
67	Fig. 5B, top	Chi-square	Extinction class	3	Chi-square	85.29	<0.0001			3-4 mice
68	Fig. 5B, middle	Chi-square	Extinction class	3	Chi-square	78.29	<0.0001			3-4 mice
69	Fig. 5B, bottom	Chi-square	Extinction class	3	Chi-square	73.77	<0.0001			3-4 mice
70	Fig. 5C	Linear regression	Fraction of Acq/Ext1/Ext3 neurons x extinction rate, saline	(1, 5)	F-statistic/Beta 0/R2	11.66/1.119 ± .3275/0.6999	0.0189			7 mice
71	Fig. 5D, top	Wilcoxon rank-sum	Median ≠ 0		Sum of signed ranks	Rap 1 -1004; Rap3 1576; Slo1 28; Slo3 152	.0001; <0.0001; .6215; .0032			60 neurons (Rap), 20 (Slow)
72	Fig. 5D, bottom	Two-Way RM ANOVA	Extinction class	(1,78)	Two-Way RM ANOVA	0.6696	0.4157			60 (Rap), 20(slow)
			Time	(1,78)		21.95	<0.0001	Sidak	Rapid: <0.0001	
			Interaction	(1,78)		8.879	0.0038	Sidak	Ext3: 0.0342	
73	Fig. 5E, top	Wilcoxon rank-sum	Median ≠ 0		Sum of signed ranks	Rap 1 189; Rap3 -89; Slo1 -384; Slo3 -388	0.0013; .1560; .1430; .1250			22 (rap),. 34 (slow)
74	Fig. 5E, bottom	Two-Way RM ANOVA	Extinction class	(1,54)	Two-Way RM ANOVA	5.533	0.0223	Sidak	Ext1: <0.0001	22 (rap),. 34 (slow)
			Time	(1,54)		35.24	<0.0001	Sidak	Rapid: <0.0001	
			Interaction	(1,54)		27.85	<0.0001			
75	Fig. 5F, top	Wilcoxon rank-sum	Median ≠ 0		Sum of signed ranks	Rap 1 48.00; Rap3 102; Slo1 371; Slo3 -233	0.2312; 1.0063; 0.0359; 0.001			16 neurons (Rap), 45 (Slow)
76	Fig. 5F, bottom	Two-Way RM ANOVA	Extinction class	(1,59)	Two-Way RM ANOVA	2.34	0.1314			16 neurons (Rap), 45 (Slow)
			Time	(1,59)		11.56	0.0012	Sidak	Rapid: 0.0137	
			Interaction	(1,59)		1.994	0.1632			
77	Fig. 6B, top	Chi-square	Group	3	Chi-square	Res vs. Sal: 19.09; Res v Nonres: 6.433; Nonres v sal: 12.04	Res vs. Sal 0.0003, Res v nonres: 0.0923; Nonres v sal: 0.0072			3-7 mice
78	Fig. 6B, middle	Chi-square	Group	3	Chi-square	Res vs. Sal:5.470; Res v Nonres: 2.487; Nonres v sal: 32.49	Res vs. Sal 0.1404, Res v nonres: 0.4776; Nonres v sal: 0.0089			3-7 mice
79	Fig. 6B, bottom	Chi-square	Group	3	Chi-square	Res vs. Sal: 16.25; Res v Nonres: .2203; Nonres v sal: 33.49	Res vs. Sal 0.001, Res v nonres: 0.9473; Nonres v sal: 0.0004			3-7 mice
80	Fig. 6C, top	Wllcoxon rank-sum	Median = 0		sum of signed ranks	R1: -1849, R3: -1794, N1 -1415, N3 -1173, S1 -151, S3 -123	R1 <0.0001, R3 <0.0001, N1 <0.0001, N3 <0.0001, S1 < 0.0001, S3 0.0021			63 neurons (R), 53 neurons (N), 17 neurons (S)
81	Fig. 6C, bottom	Two Way RM ANOVA	Group	(2, 130)	F-statistic	4.734	0.0104	Sidak: Ext1, Ext3	Ext1: Res vs. Non 0.0155; Res vs. Sal 0.9998; Non vs. Sal 0.1974 Ext3: Res vs. Non 0.0199; Res vs. Sal 0.9992; Non vs. Sal 0.2398	63 neurons (R), 53 neurons (N), 17 neurons (S)
			Time	(1, 130)		2.965	0.0875			
			Interaction	(2, 130)		0.01344	0.9866			
82	Fig. 6D, top	Wllcoxon rank-sum	Median = 0		sum of signed ranks	R1: 493, R3: 489, N1 754, N3 326, S1 183, S3 5	R1 0.0010, R3 0.0011, N1 <0.0001, N3 0.0856, S1 0.0007, S3 0.9383			41 neurons (R), 47 neurons (N), 21 neurons (S)
83	Fig. 6D, bottom	Two Way RM ANOVA	Group	(2, 106)		1.845	0.163			41 neurons (R), 47 neurons (N), 21 neurons (S)
			Time	(1, 106)		20.77	0.0104	Sidak: Res, Non-Res, Sal	Res: Ext1 vs. Ext3 0.0488; Non: Ext1 vs. Ext3 0.2563; Sal: Ext1 vs. Ext3 0.0020	
			Interaction	(2, 106)	F-statistic	1.961	0.9866			

Row	Figure	Statistical Model	Variable	Degrees of Freedom (DFn, DFd)	Parameter(s)	Paramter value	p-value	Multiple comparisons? (Sidak test)	p-value	n per group
84	Fig. 6E, top	WIlcoxon rank-sum	Median = 0		sum of signed ranks	R1: 28, R3: 1784, N1 355, N3 941, S1 -1004, S3 1576	R1 0.9214, R3 <0.0001, N1 0.0525, N3 <0.0001, S1 0.0001, S3 < 0.0001			60 neurons (R), 46 neurons (N), 60 neurons (S)
85	Fig. 6E, bottom	Two Way RM ANOVA	Group	(1, 163)		5.424	0.0052	Ext1, Ext3	Ext3: Res vs. Non <0.0001; Res vs. Sal 0.0039; Sal v non .3349	60 neurons (R), 46 neurons (N), 60 neurons (S)
			Time	(2, 163)		112.4	<0.0001	Res, Non-Res, Sal	Res: <0.0001; Non:0.0083; Sal: <0.0001	
			Interaction	(2, 163)	F-statistic	8.183	0.0004			
86	Fig. 6F, top	WIlcoxon rank-sum	Median = 0		sum of signed ranks	R1: -307, R3: -465, N1 -48, N3 -328, S1 189, S3 -89	R1 0.0077, R3 <0.0001, N1 0.5979, N3 <0.0001, S1 0.156, S3 < 0.0001			34 neurons (R), 28 neurons (N), 22 neurons (S)
87	Fig. 6F, bottom	Two Way RM ANOVA	Group	(2, 81)		6.869	0.0004	Ext1, Ext3	Ext1: Res v npn: Res vs. Sal <0.0001; Non vs. Sal <0.0001	34 neurons (R), 28 neurons (N), 22 neurons (S
			Time	(1, 81)		22.41	<0.0001	Res, Non-Res, Sal	Res Ext1 vs. Ext3: 0.0744; Non: Ext1 vs. Ext3 0.0136 Sal: Ext1 vs. Ext3 <0.0001	
			Interaction	(2, 81)	F-statistic	0.6691	<0.0001			
88	Fig. 6G, top	WIlcoxon rank-sum	Median = 0		sum of signed ranks	R1: -210, R3: 16, N1 -187, N3 -19, S1 -119, S3 31	R1 <0.0001, R3 0.0049, N1 0.0005, N3 0.7593, S1 0.4235, S3 0.4874			20 neurons (R), 21 neurons (N), 17 neurons (S)
89	Fig. 6G, bottom	Two Way RM ANOVA	Group	(2, 81)		8.81	0.5472	Ext1, Ext3	Res: Ext1 vs. Ext3 <0.0001; Non: Ext1 vs. Ext3 0.0364; Sal: Ext1 vs. Ext3 <0.0001	20 neurons (R), 21 neurons (N), 17 neurons (S)
			Time	(1, 81)		75.07	<0.0001	Res, Non-Res, Sal	Ext3 Res vs. Non: 0.0057	
			Interaction	(2, 81)	F-statistic	0.6069	0.0005			
90	Fig. 6H, top	WIlcoxon rank-sum	Median = 0		sum of signed ranks	R1: 693, R3: 1035, N1 368, N3 490, S1 93, S3 93	R1 <0.0001, R3 <0.0001, N1 0.0003, N3 <0.0001, S1 0.4016, S3 0.0016			45 neurons (R), 32 neurons (N), 14 neurons (S)
91	Fig. 6H, bottom	Two Way RM ANOVA	Group	(2, 55)		3.698	0.0287	Ext1, Ext3	Non vs. Sal 0.0134	45 neurons (R), 32 neurons (N), 14 neurons (S)
			Time	(1, 55)		0.9934	0.3216	Res, Non-Res, Sal		
			Interaction	(2, 55)	F-statistic	0.9202	0.4022			
92	Fig. 6I, top	WIlcoxon rank-sum	Median = 0		sum of signed ranks	R1: -165, R3: 69, N1 265, N3 263, S1 48, S3 102	R1 0.0255, R3 0.3666, N1 0.0032, N3 0.0035, S1 0.2312, S3 0.0063			25 neurons (R), 29 neurons (N), 16 neurons (S))
93	Fig. 6I, bottom	Two Way RM ANOVA	Group	(2, 112)		5.609	<0.0001	Ext1, Ext3	Ext1: Res vs. Non 0.0156; Res vs. Sal 0.0178 Ext3: Res vs. Sal 0.0086	25 neurons (R), 29 neurons (N), 16 neurons (S)
			Time	(1, 112)		16.18	0.0038	Res, Non-Res, Sal	Res: Ext1 vs. Ext3 0.002; Sal: Ext1 vs. Ext3 0.0039	
			Interaction	(2, 112)	F-statistic	0.9663	0.0768			
94	Fig. 7B, top	WIlcoxon rank-sum	Median = 0		sum of signed ranks	R1: -8126, R3: -4531, N1 -3852, N3 -2972, SR1-422 SR3 -324 SS1 194, SS3 548	R1<0.0001, R3 <0.0001, N1 <0.0001, N3 0.0006, SR1 0.3670, SR3 0.3690; SS1 0.6390; SS3 0.1824			145 neurons (R), 128 neurons (N), 72 neurons (Rap), 79 neurons (Slow)
95	Fig. 7B, bottom	Two Way RM ANOVA	Group	(3, 420)		12.99	<0.0001	Ext1, Ext3	Ext1: Res vs. Non 0.0003; Res vs. Rapid <0.0001; Res vs. Slow <0.0001; Ext3: Res vs. Rapid 0.0052; Res vs. Slow 0.0004;	145 neurons (R), 128 neurons (N), 72 neurons (Rap), 79 neurons (Slow)
			Time	(1, 420)		5.524	0.0192			
			Interaction	(3, 420)	F-statistic	1.178	0.1625			
96	Fig. 7C, top	WIlcoxon rank-sum	Median = 0		sum of signed ranks	R1: 2229, R3: 4645, N1 4941, N3 2719, SR1 2192 SR3 1483, SS1 194, SS3 548	R1 0.0276, R3 <0.0001, N1 <0.0001, N3 0.0001, SR1 <0.0001, SR3 0.0001, SS1 0.6390, SS3 0.6390,			145 neurons (R), 137 neurons (N), 73 neurons (Rap), 79 neurons (Slow)
97	Fig. 7C, bottom	Two Way RM ANOVA	Group	(3, 426)		8.33	<0.0001	Ext1, Ext3	Ext1: Res v Rap: 0.0003; Non v Rap: 0.0062; Rap v Slow: <0.0001	145 neurons (R), 137 neurons (N), 73 neurons (Rap), 79 neurons (Slow)
			Time	(1, 426)		0.9501	0.3302			
			Interaction	(3, 426)	F-statistic	1.251	0.2909			
98	Fig. 7D, top	WIlcoxon rank-sum	Median = 0		sum of signed ranks	R1: 157, R3: 9921, N1 2606, N3 5870, S1 -1279, S3 5038, S1 1339, S3 1129	R1 0.8840, R3 <0.0001, N1 0.0018, N3 <0.0001, S1 0.0407, S3 <0.0001, S1 0.0821, S3 <.0002			145 neurons (R), 137 neurons (N), 105 neurons (Rap); 65 (Slow
			Group	(2, 390)		8.085	<0.0001	Ext1, Ext3	Ext3: Res vs. Non <0.0001; Res vs. Rap 0.0365; Res v Slow: <0.0001; Non v Rap: 0.0116; Rap v slow: 0.0003	

Row	Figure	Statistical Model	Variable	Degrees of Freedom (DFn, DFd)	Parameter(s)	Paramter value	p-value	Multiple comparisons? (Sidak test)	p-value	n per group
99	Fig. 7D, bottom	Two Way RM ANOVA	Time	(1, 390)		136.5	<0.0001	Res, Non-Res, Sal	Res: Ext1 vs. Ext3 <0.0001; Non: Ext1 vs. Ext3 <0.0001; Sal: Ext1 vs. Ext3 <0.0001	145 neurons (R), 137 neurons (N), 105 neurons (Rap); 65 (Slow
			Interaction	(2, 390)	F-statistic	8.3	<0.0001			
100	Fig. 7E	Linear regression	Activity of shock responsive Acq dom neurons x freezing late Ext3 psil	(1,12)	F-statistic/Beta 0/R2	7.3591/ 24.27±8.947/0.3801	0.0189			7 mice
101	Fig. 7F	Linear regression	Activity of nonoverlapping shock responsive Ext3-dom neurons x freezing late ext3	(1, 12)	F-statistic/Beta 0/R2	15.47/-16.58±4.214/ 0.5632	0.0002			21 mice
102	Supp Fig. 1A panel 1	Two Way RM ANOVA	Treatment	(1,50)		2.165	0.1474			22 psil, 29 sal
			Time	(7, 350)		0.6103	0.7475			
			Interaction	(7, 350)	F-statistic	0.6835	0.686			
103	Supp Fig. 1A panel 2	Two Way RM ANOVA	Treatment	(1,50)		2.939	0.0525			22 psil, 29 sal
			Time	(7, 350)		155.8	<0.0001			
			Interaction	(7, 350)	F-statistic	0.6591	0.7067			
104	Supp Fig. 1A panel 3	Two Way RM ANOVA	Treatment	(1,50)		4.161	0.0467	Trial 3: 0.0359, Trial 4: 0.0354		22 psil, 29 sal
			Time	(7, 350)		7.14	<0.0001			
			Interaction	(7, 350)	F-statistic	2.289	0.0465			
105	Supp Fig. 1A panel 4	Two Way RM ANOVA	Treatment	(1,50)		5.199	0.016	Trials	Sal vs. Psil: Trial 2: 0.0182, Trial 4: 0.0217	22 psil, 29 sal
			Time	(7, 350)		2.067	0.0701			
			Interaction	(7, 350)	F-statistic	2.848	0.0269			
106	Supp Fig. 1A panel 5	Two Way RM ANOVA	Treatment	(1,50)		1.318	0.1581			22 psil, 29 sal
			Time	(7, 350)		3.6585	0.0035			
			Interaction	(7, 350)	F-statistic	0.5474	0.5562			
107	Supp Fig. 1B	Two Way RM ANOVA	Sex	(1,27)		0.1026	0.7512			7-18 mice
			Time	(27, 243)		28.88	<0.0001			
			Interaction	(27, 243)	F-statistic	1.034	0.4132			
108	Supp Fig. 1C	Two Way RM ANOVA	Sex	(1, 20)		0.4265	0.5211			7-18 mice
			Time	(9, 180)		42.41	<0.0001			
			Interaction	(9, 180)	F-statistic	0.6221	0.7772			
109	Supp Fig. 1D	Two Way RM ANOVA	Treatment	(1,4)		0.1253	0.7412			9-17 mice
			Time	(9,36)		4.254	0.008			
			Interaction	(9,36)	F-statistic	1.457	0.2355			
110	Supp Fig. 1E	Two Way RM ANOVA	Treatment	(1,49)		1.39	0.2441			7-18 mice
			Time	(1,49)		23.67	<0.0001	Baseline vs. trace	Sal: <0.0001; Psil 0.0160	
			Interaction	(1,49)	F-statistic	1.216	0.2755			
111	Supp Fig. 1F	Two Way RM ANOVA	Treatment	(1,49)		3.314	0.0829			7-18 mice
			Time	(1,49)		1.247	0.2696			
			Interaction	(1,49)	F-statistic	0.4218	0.5191			
112	Supp Fig. 2B	Two Way RM ANOVA	Treatment	(12, 68)		0.8675	0.4727			3 mice
			Time	(4, 68)		8.696	<0.0001			
			Interaction	(17, 68)	F-statistic	0.5662	0.8615			
113	Supp Fig. 2C, Panel 1	Two Way ANOVA	Treatment	(1,17)		1.261	0.277			7-18 mice
			Extinction Class	(1,17)		1.225	0.2838			
			Interaction	(1,17)	F-statistic	0.4269	0.5222			
114	Supp Fig. 2C, Panel 2	Two Way ANOVA	Treatment	(1,17)		0.04233	0.8394			7-18 mice
			Extinction Class	(1,17)		0.3822	0.5446			
			Interaction	(1,17)	F-statistic	0.01151	0.9158			
115	Supp Fig. 2C, Panel 3	Two Way ANOVA	Treatment	(1,17)		0.6713	0.1651			7-18 mice
			Extinction Class	(1,17)		0.6673	0.4253			
			Interaction	(1,17)	F-statistic	2.104	0.4239			
116	Supp Fig. 2C, Panel 4	Two Way ANOVA	Treatment	(1,17)		0.1883	0.6698			7-18 mice
			Extinction Class	(1,17)		0.3438	0.5654			
			Interaction	(1,17)	F-statistic	4.24	0.0551			
117	Supp Fig. 2C, Panel 5	Two Way ANOVA	Treatment	(1,17)		0.1476	0.7056			7-18 mice
			Extinction Class	(1,17)		0.6509	0.4309			
			Interaction	(1,17)	F-statistic	0.006763	0.9354			
118	Supp Fig. 2E, Panel 1	Two Way ANOVA	Treatment	(1,17)		1.666	0.214			7-18 mice
			Extinction Class	(1,17)		0.485	0.4956			
			Interaction	(1,17)	F-statistic	0.299	0.5916			
119	Supp Fig. 2E, Panel 2	Two Way ANOVA	Treatment	(1,17)		1.932	0.1825			7-18 mice
			Extinction Class	(1,17)		0.5825	0.4558			
			Interaction	(1,17)	F-statistic	0.7397	0.4017			
			Treatment	(1,17)		3.089	0.0968			

Row	Figure	Statistical Model	Variable	Degrees of Freedom (DFn, DFd)	Parameter(s)	Paramter value	p-value	Multiple comparisons? (Sidak test)	p-value	n per group
120	Supp Fig. 2E, Panel 3	Two Way ANOVA	Extinction Class	(1,17)		0.02798	0.8691			
			Interaction	(1,17)	F-statistic	0.8103	0.3806			7-18 mice
121	Supp Fig. 2E, Panel 4	Two Way ANOVA	Treatment	(1,17)		4.519	0.0485			
			Extinction Class	(1,17)		0.4693	0.5025			
			Interaction	(1,17)	F-statistic	0.06964	0.795			7-18 mice
122	Supp Fig. 2E, Panel 5	Two Way ANOVA	Treatment	(1,17)		0.3512	0.266			
			Extinction Class	(1,17)		0.1452	0.7079			
			Interaction	(1,17)	F-statistic	1.323	0.5612			7-18 mice
123	Supp Fig. 2G, Panel 1	Two Way ANOVA	Treatment	(1,17)		3.0676	0.0979			
			Extinction Class	(1,17)		5.674	0.0292			
			Interaction	(1,17)	F-statistic	13.91	0.0017			7-18 mice
124	Supp Fig. 2G, Panel 2	Two Way ANOVA	Treatment	(1,17)		0.2305	0.6373			
			Extinction Class	(1,17)		1.436	0.2472			
			Interaction	(1,17)	F-statistic	0.8092	0.3809			7-18 mice
125	Supp Fig. 2G, Panel 3	Two Way ANOVA	Treatment	(1,17)		2.208	0.5157			
			Extinction Class	(1,17)		0.003729	0.952			
			Interaction	(1,17)	F-statistic	0.4406	0.1556			7-18 mice
126	Supp Fig. 2G, Panel 4	Two Way ANOVA	Treatment	(1,17)		1.114	0.306			
			Extinction Class	(1,17)		1.644	0.217			
			Interaction	(1,17)	F-statistic	3.203	0.0913			7-18 mice
127	Supp Fig. 2G, Panel 5	Two Way ANOVA	Treatment	(1,17)		0.009515	0.9234			
			Extinction Class	(1,17)		0.002574	0.9601			
			Interaction	(1,17)	F-statistic	0.9156	0.3521			7-18 mice
128	Supp Fig. 2I, Panel 1	Two Way ANOVA	Treatment	(1,17)		1.666	0.214			
			Extinction Class	(1,17)		0.485	0.4956			
			Interaction	(1,17)	F-statistic	0.299	0.5916			7-18 mice
129	Supp Fig. 2I, Panel 2	Two Way ANOVA	Treatment	(1,17)		1.932	0.1825			
			Extinction Class	(1,17)		0.5825	0.4558			
			Interaction	(1,17)	F-statistic	0.7397	0.4017			7-18 mice
130	Supp Fig. 2I, Panel 3	Two Way ANOVA	Treatment	(1,17)		3.089	0.0968			
			Extinction Class	(1,17)		0.02798	0.8691			
			Interaction	(1,17)	F-statistic	0.8103	0.3806			7-18 mice
131	Supp Fig. 2I, Panel 4	Two Way ANOVA	Treatment	(1,17)		4.519	0.0485			
			Extinction Class	(1,17)		0.4693	0.5025			
			Interaction	(1,17)	F-statistic	0.06964	0.795			7-18 mice
132	Supp Fig. 2I, Panel 5	Two Way ANOVA	Treatment	(1,17)		0.3512	0.5612			
			Extinction Class	(1,17)		0.1452	0.7079			
			Interaction	(1,17)	F-statistic	1.323	0.266			7-18 mice
133	Supp Fig. 3A	Two Way RM ANOVA	Sex	(3,17)		0.6941	0.5683			
			Time	(59, 1003)		0.8867	0.7145			
			Interaction	(17, 1003)	F-statistic	0.8	0.6984			7 mice
134	Supp Fig. 3B	Two Way RM ANOVA	Sex	(3,17)		0.3718	0.7744			
			Time	(59, 1003)		3.18	<0.0001			
			Interaction	(17, 1003)	F-statistic	1.014	0.4399			7 mice
135	Supp Fig. 3C	Two Way RM ANOVA	Sex	(3,17)		1.329	0.2978			
			Time	(59, 1003)		1.021	0.4338			
			Interaction	(17, 1003)	F-statistic	1.52	<0.0001			7 mice
136	Supp Fig. 3D	Two Way RM ANOVA	Sex	(3,17)		1.741	0.5685			
			Time	(59, 1003)		1.457	0.0155			
			Interaction	(17, 1003)	F-statistic	0.9772	0.1966			7 mice
137	Supp Fig. 3E	Two Way RM ANOVA	Sex	(3,17)		0.327	0.8059			
			Time	(59, 1003)		1.255	0.0973			
			Interaction	(17, 1003)	F-statistic	1.136	0.1261			7 mice
138	Supp Fig. 5B	One Way RM ANOVA	Time	(9,20)	F-statistic	0.6529	0.5091			3 mice
139	Supp. Fig. 5D	One Way ANOVA	Group	(3, 396)	F-statistic	55.71	<0.0001	Compare to non-shock	All comparisons: <0.0001	100 iterations
140	Supp. Fig. 5E	Chi-square	Group (Non-shock v. Saline)	3	Chi-square	23.85	<0.0001			
141	Supp. Fig. 5F	Chi-square	Group (Non-shock v. Saline)	3	Chi-square	37.73	<0.0001			
142	Supp. Fig. 5G	Chi-square	Group (Non-shock v. Saline)	3	Chi-square	56.13	<0.0001			
			Group	(1, 227)		10.76	0.0012	Sal vs. Nonshock	Ext1: 0.0149, Ext3: 0.0061	

Row	Figure	Statistical Model	Variable	Degrees of Freedom (DFn, DFd)	Parameter(s)	Paramter value	p-value	Multiple comparisons? (Sidak test)	p-value	n per group
143	Supp Fig. 5H	Two Way RM ANOVA	Time	(1, 227)		0.1684	0.6819			151 saline, 78 non-shock neurons
			Interaction	(1, 227)	F-statistic	0.08495	0.771			
144	Supp Fig. 5I	Two Way RM ANOVA	Group	(1, 224)		2.25	0.238			158 saline, 69 non-shock neurons
			Time	(1, 224)		1.135	0.2879			
			Interaction	(1, 224)	F-statistic	2.25	0.135			
145	Supp Fig. 5J	Two Way RM ANOVA	Group	(1, 256)		1.551	0.1948			175 saline, 83 non-shock neurons
			Time	(1, 256)		76.18	<0.0001			
			Interaction	(1, 256)	F-statistic	6.403	0.0201	Sal vs. Nonshock	Ext1: 0.9611, Ext3: 0.0337	
146	Supp. Fig. 6H, left	Two Way RM ANOVA	Group	(2, 479)		12.11	<0.0001	Ext1, Ext3	Ext1: Res vs. Non 0.0003; Res vs. Sal < 0.0001 Non vs. Sal 0.3995 Ext3: Res vs. Non 0.8865; Res vs. Sal 0.0034; Non vs. Sal 0.0322	142 neurons (R), 131 neurons (N), 167 neurons (S)
			Time	(1, 479)		14.01	0.0002	Res, Non-Res, Sal	Res: < 0.0001; Non: >0.9999 ; Sal: 0.2474	
			Interaction	(2, 479)	F-statistic	6	0.0022			
147	Supp. Fig. 6H, middle	Two Way RM ANOVA	Group	(2, 481)		0.3818	0.6829			178 neurons (R), 148 neurons (N), 158 neurons (S)
			Time	(1, 481)		0.2102	0.6468			
			Interaction	(2, 481)	F-statistic	2.424	0.0896			
148	Supp. Fig. 5H, right	Two Way RM ANOVA	Group	(2, 484)		2.864	<0.0001	Ext1, Ext3	Ext1: Res vs. Non 0.9469; Res vs. Sal 0.9972 Non vs. Sal 0.9840 Ext3: Res vs. Non <0.0001; Res vs. Sal 0.0374; Non vs. Sal 0.1111	171 neurons (R), 144 neurons (N), 171 neurons (S)
			Time	(1, 484)		122.8	<0.0001	Res, Non-Res, Sal	Res: < 0.0001; Non: 0.0076 ; Sal:< 0.0001	
			Interaction	(2, 484)	F-statistic	10.13	0.058			